# Homologs of Circadian Clock Proteins Impact the Metabolic Switch Between Light and Dark Growth in the Cyanobacterium *Synechocystis* sp. PCC 6803

Nina M. Scheurer[1†], Yogeswari Rajarathinam[2†], Stefan Timm[3], Christin Köbler[1], Joachim Kopka[2], Martin Hagemann[3] and Annegret Wilde[1*]

[1] Institute of Biology III, University of Freiburg, Freiburg, Germany, [2] Applied Metabolome Analysis, Department of Molecular Physiology, Max Planck Institute of Molecular Plant Physiology, Potsdam, Germany, [3] Department of Plant Physiology, University of Rostock, Rostock, Germany

The putative circadian clock system of the facultative heterotrophic cyanobacterial strain *Synechocystis* sp. PCC 6803 comprises the following three Kai-based systems: a KaiABC-based potential oscillator that is linked to the SasA-RpaA two-component output pathway and two additional KaiBC systems without a cognate KaiA component. Mutants lacking the genes encoding the KaiAB1C1 components or the response regulator RpaA show reduced growth in light/dark cycles and do not show heterotrophic growth in the dark. In the present study, the effect of these mutations on central metabolism was analyzed by targeted and non-targeted metabolite profiling. The strongest metabolic changes were observed in the dark in Δ*rpaA* and, to a lesser extent, in the Δ*kaiAB1C1* mutant. These observations included the overaccumulation of 2-phosphoglycolate, which correlated with the overaccumulation of the RbcL subunit in the mutants, and taken together, these data suggest enhanced RubisCO activity in the dark. The imbalanced carbon metabolism in the Δ*rpaA* mutant extended to the pyruvate family of amino acids, which showed increased accumulation in the dark. Hence, the deletion of the response regulator *rpaA* had a more pronounced effect on metabolism than the deletion of the *kai* genes. The larger impact of the *rpaA* mutation is in agreement with previous transcriptomic analyses and likely relates to a KaiAB1C1-independent function as a transcription factor. Collectively, our data demonstrate an important role of homologs of clock proteins in *Synechocystis* for balanced carbon and nitrogen metabolism during light-to-dark transitions.

Keywords: circadian clock, *Synechocystis*, carbon metabolism, RpaA, diurnal metabolic switch
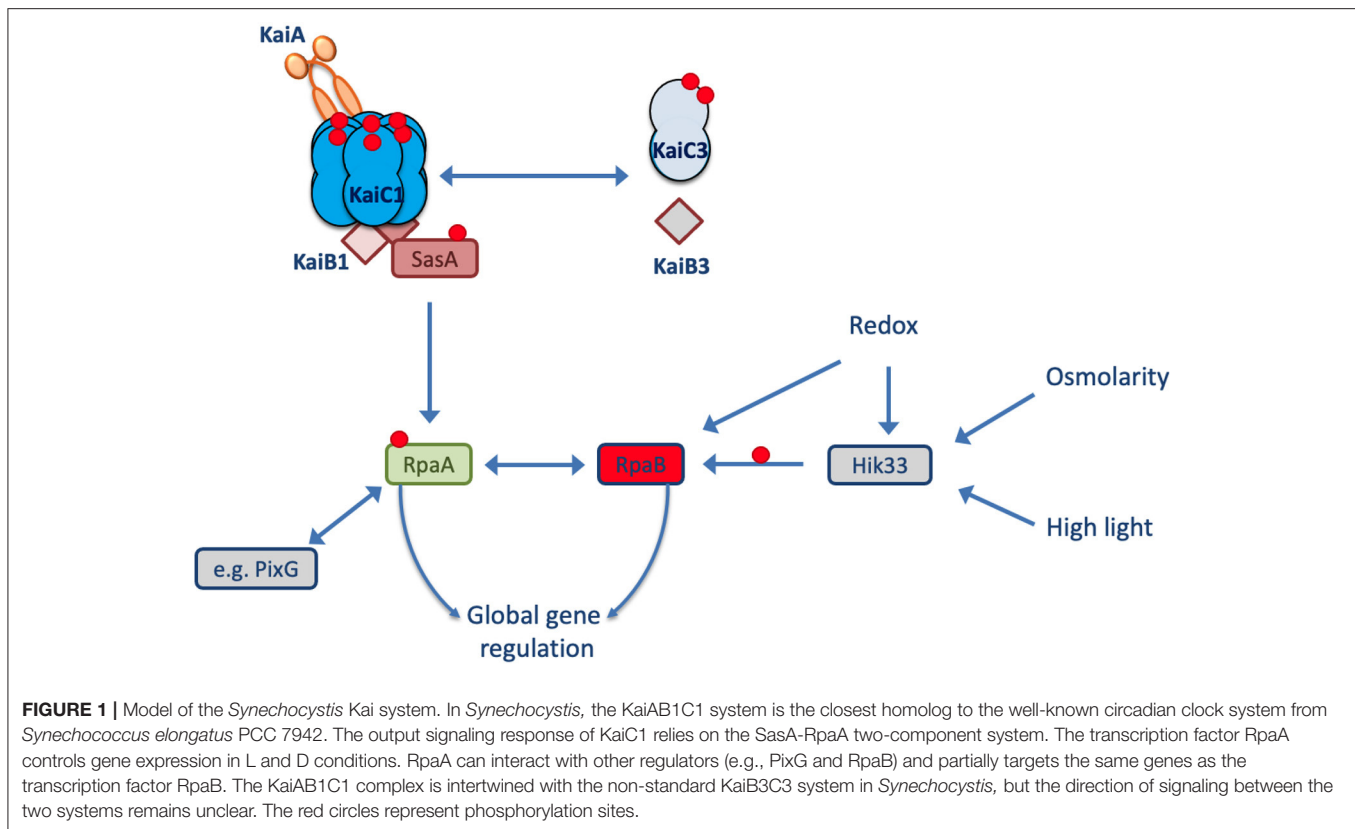
## INTRODUCTION

Most organisms on Earth experience daily environmental changes. Similar to eukaryotic organisms, photosynthetic cyanobacteria evolved a circadian clock system to respond to predictable fluctuations of light (L) and darkness (D) in a day-night cycle. The freshwater obligate photoautotrophic cyanobacterium *Synechococcus elongatus* PCC 7942 is a model strain used in cyanobacterial circadian research (Cohen and Golden, 2015). Research based on this cyanobacterium established the proteins KaiA, KaiB, and KaiC as the core oscillators of the clock system (Ishiura et al., 1998; Iwasaki et al., 1999). KaiC performs autokinase, autophosphatase and ATPase functions that are modulated by interaction with KaiA and KaiB. The rhythmic phosphorylation pattern of KaiC functions as a marker of the clock phase and controls rhythmic gene expression. To transfer time information to cellular functions, the oscillator is linked to a two-component regulatory system consisting of the histidine kinase SasA and the DNA-binding response regulator RpaA (Gutu and O'Shea, 2013). During the day, KaiC is progressively phosphorylated. In its highly phosphorylated state, KaiC activates SasA autophosphorylation activity, resulting in the subsequent phosphorylation of RpaA. In *Synechococcus elongatus* PCC 7942, phosphorylated RpaA acts as a repressor of dawn-peaking genes and activator of dusk-peaking genes, and the deletion of *rpaA* leads to the arrest of cells in a dawn-like state (Markson et al., 2013). Although mutations in the KaiABC circadian oscillator do not strongly impair the L/D growth of *Synechococcus elongatus* PCC 7942, the Δ*rpaA* strain is unable to grow in a L/D cycle because it loses viability in D. The described phenotypes of the *Synechococcus rpaA* mutant strain include imbalances in redox regulation and the accumulation of carbon storage compounds (Diamond et al., 2017; Puszynska and O'Shea, 2017).

*Synechocystis* sp. PCC 6803 (hereafter *Synechocystis*) is another frequently used model strain that, in contrast to *Synechococcus elongatus* PCC 7942, can use glucose for mixotrophic and heterotrophic growth and can tolerate high salinities (Rippka et al., 1979; Kirsch et al., 2019). It contains the KaiA, KaiB1, and KaiC1 proteins with high similarity to the *Synechococcus* oscillator proteins. Moreover, the *Synechocystis* genome encodes two additional copies of the *kaiC* (*kaiC2* and *kaiC3*) and *kaiB* (*kaiB2* and *kaiB3*) genes (Wiegard et al., 2013). Köbler et al. (2018) showed that the homologous SasA-RpaA two-component system of *Synechocystis* interacts only with KaiC1 but not KaiC2 or KaiC3. This specificity of the SasA-RpaA system for KaiC1 suggests that the additional Kai components of *Synechocystis* may use different output elements (**Figure 1**).

True circadian oscillations, which continue after shifting the cells into a constant environment, may not be active in *Synechocystis*, but robust transcriptional rhythmicity in a diurnal light regime has been described (Beck et al., 2014). Diurnal oscillations depend on daily recurring external stimuli sustaining a 24 h period. While a *Synechocystis* Δ*kaiC3* mutant shows no growth defect in a L/D cycle, the deletion of the *kaiB2C2* operon is lethal even in constant light (Dörrich et al., 2014). In contrast, the deletion of the *kaiAB1C1* gene cluster and the

response regulator gene *rpaA,* caused defects in cell viability in a 12-h L/12-h D cycle, especially under mixotrophic conditions. Furthermore, in complete D, neither mutant strain was able to grow heterotrophically, whereas wild-type growth was slow but observable (Dörrich et al., 2014; Köbler et al., 2018). Surprisingly, DNA microarray analyses of both mutant strains demonstrated a considerable difference in their transcriptome responses to a switch from D to L. The overlap in the transcriptional responses between the mutants was only 50% in studies performed under identical conditions with a similar microarray design (Dörrich et al., 2014; Köbler et al., 2018). The overlap in the transcriptional changes contained mRNAs encoding regulatory proteins, such as ribonuclease E (*rne*), phytochrome 1 (*cph1*), and the sigma factor SigE (*sigE*). Furthermore, the Δ*kaiAB1C1* and Δ*rpaA* mutations affected mRNAs of both *gnd* encoding the 6-phosphogluconate dehydrogenase and *talB* encoding the transaldolase. These enzymes are a part of the oxidative pentose phosphate pathway (OPPP), which is activated during the night and converts glucose-6-phosphate (glucose-6P) into pentose- and other sugar phosphates, thereby providing NADPH reduction equivalents (Makowka et al., 2020). In contrast to Gnd, TalB is also active in the Calvin-Benson-Bassham (CBB) cycle during the L phase. In addition to the common effects of the two mutants, the Δ*rpaA* mutant activates in L the transcription of many genes known to be involved in acclimation to low inorganic carbon ($C_i$) concentrations, i.e., bicarbonate and $CO_2$. In D, in Δ*rpaA,* but not Δ*kaiAB1C1,* we observed a decreased transcript accumulation of two enzymes (PhaC/PhaE) involved in NADPH-consuming synthesis (via acetoacetyl-CoA reductase PhaB) of the storage compound polyhydroxybutyrate (PHB), which is produced from glycogen under unbalanced nutrient conditions in response to nitrogen starvation (Koch et al., 2019, 2020a). Werner et al. (2019) performed very detailed metabolite profiling during a sinusoidal diurnal cycle with a light intensity peak in the middle of the day. These authors found highly concerted oscillations of metabolites across the cycle, verifying that *Synechocystis* performs carbon fixation and protein and nucleotide synthesis during the day. Surprisingly, the authors reported a sharp oscillation in the amount of insoluble carbohydrates at approximately the L-to-D switch. Cyanobacteria store fixed carbon mainly as glycogen, which is then degraded at night using OPPP. Further glycolytic routes, including the Entner-Doudoroff (ED) pathway, which branches off the OPPP, and the Embden-Meyerhof-Parnas (EMP) pathway, have been identified (Chen et al., 2016).

The current study aims to investigate the role of the main homologs of circadian clock proteins on the L and D metabolism in *Synechocystis*. Though *Synechocystis* mutants lacking the *kaiAB1C1* operon or the *rpaA* gene show a similar growth defect in a L/D cycle and in heterotrophic growth in D, previous transcriptomic analyses suggest major differences in gene expression between these two mutants. To better understand the specific impact of the putative KaiA1BC1 oscillator in comparison to the output regulator RpaA on metabolism, we measured primary metabolites in the middle of the D and L phases by targeted and untargeted metabolic profiling. These are the same time

**FIGURE 1 |** Model of the *Synechocystis* Kai system. In *Synechocystis,* the KaiAB1C1 system is the closest homolog to the well-known circadian clock system from *Synechococcus elongatus* PCC 7942. The output signaling response of KaiC1 relies on the SasA-RpaA two-component system. The transcription factor RpaA controls gene expression in L and D conditions. RpaA can interact with other regulators (e.g., PixG and RpaB) and partially targets the same genes as the transcription factor RpaB. The KaiAB1C1 complex is intertwined with the non-standard KaiB3C3 system in *Synechocystis,* but the direction of signaling between the two systems remains unclear. The red circles represent phosphorylation sites.

points which were investigated in the previous transcriptome analyses of the Δ*kaiAB1C1* and Δ*rpaA* mutants. The identified differences in the metabolic responses clearly indicate that mainly the lack of the RpaA regulator impacts primary metabolism and the metabolic switch between L and D growth.

## MATERIALS AND METHODS

### Cyanobacterial Strains, Culture, and Sampling Conditions

For standard cultivation, the *Synechocystis* sp. PCC 6803 wild-type (PCC-M, resequenced, Trautmann et al., 2012) and mutant strains were grown photoautotrophically under constant illumination with 75 $\mu$mol photons m$^{-2}$ s$^{-1}$ white light at 30°C in BG11 medium (Rippka et al., 1979) supplemented with 10 mM TES buffer (pH 8) in flasks. For the L/D experiments, the precultures were grown in constant light and diluted to OD$_{750}$ 0.4–0.6 before transfer to alternating 12-h L/12-h D cycles with 75 $\mu$mol photons m$^{-2}$ s$^{-1}$ during the L phase. Depending on the experimental setup, air was supplemented with $CO_2$ (1%, v/v), and illumination was increased to 150 $\mu$mol photons m$^{-2}$ s$^{-1}$ after the liquid cultures reached an OD$_{750}$ of ∼1. The wild-type and mutant strains were cultured in triplicate. The samples were collected in the middle of the first D phase and the following L phase 5.5 h after each transition in the exponential growth phase if not described otherwise.

### RNA Isolation and Northern Blot Hybridization

The RNA isolation was performed following Pinto et al. (2009). For sampling, 20 ml of culture were filtered through a Supor-800 membrane filter (0.8 mm, Pall), vortexed in 1.6 ml PGTX for 30 s and immediately frozen in liquid nitrogen. The samples were stored at −80°C. After thawing the samples on ice, the samples were heated at 95°C for 5 min. The lysis was supported by vortexing during the incubation. After cooling the samples on ice for 5 min, the samples were incubated at room temperature (RT) for 10 min. Then, 200 $\mu$l of cold bromchloropropane (BCP) were added, vortexed for 30 s and stored at RT for 15 min. Next, the phases were separated by centrifugation at 3,100 ×g for 15 min at 4°C. The aqueous phase was transferred into a new reaction tube, and the reaction was repeated once more with 1 volume of cold BCP. The samples were centrifuged at 21,130 ×g for 15 min at 4°C, followed by precipitation with 1 volume of isopropanol and storage of the sample overnight at −20°C. The samples were centrifuged at 21,130 ×g for 1 h at 4°C, the resulting pellet was washed with 75% EtOH, and centrifugation was repeated for 10 min. The pellet was air-dried for 15 min and resuspended in 40 $\mu$l ddH$_2$O.

To separate the RNA, 10 $\mu$g were used for electrophoresis on a 1.5% denaturing agarose-formaldehyde gel. The gel was blotted onto a Roti-Nylon plus membrane (Roth). The DNA fragment used for probe generation was amplified from wild-type DNA using the oligonucleotides sbtA-fw (5$^{'}$    CAATCCCCATAAATTTCAACCAAGGAGAC    3$^{'}$)

and sbtA-rev (5′ TAATACGACTCACTATAGGGAGAGC-CAAGGGCGGCAATAACCATC 3′). The probe was produced with a Rediprime II labeling kit (GE Healthcare). Hybridization was performed as described by Dienst et al. (2008), and the signals were detected using a Typhoon FLA 9500 (GE Healthcare).

## Immunoblot Analysis of RubisCO

The wild-type and mutant cultures of *Synechocystis* were diluted to $OD_{750}$ 0.6 and cultivated in an L/D cycle. Five milliliter of WT and mutant cultures of *Synechocystis* were harvested by centrifugation at 4,000 ×g for 2 min at 4°C. After the pellet was resuspended in PBS buffer (8.6 mM $Na_2PO_4$, 1.8 mM $KH_2PO_4$, 137 mM NaCl, 2.7 mM KCl, pH 7.5), the cells were disrupted in a cell mill using glass beads. The crude extract was obtained by centrifugation at 500 ×g for 5 min at 4°C, and different protein amounts of the crude extract were subjected to SDS-PAGE. The immunodetection was performed using anti-RbcL (Agrisera, Sweden) and secondary anti-rabbit (Thermo Fisher Scientific Inc., USA) antibodies.

## Quantification of the PHB Content

The intracellular PHB content was measured as described by Taroncher-Oldenburg et al. (2000). The wild-type and mutant cultures were adjusted to $OD_{750}$ 0.2 and then grown in L/D cycles supplemented with $CO_2$ as described above. The samples were collected in the 7th L/D cycle 1 h before the L or D transitions. Approximately 15–35 ml of cell culture were harvested by centrifugation (4,000 ×g, 10 min, 4°C), washed once with $H_2O$ and dried overnight at 85°C. To break the cells and convert PHB, the pellet was boiled in 1 ml concentrated $H_2SO_4$ for 1 h. Then, 100 µl were transferred to 900 µl of 0.014 M $H_2SO_4$. To pellet the cell debris, the sample was centrifuged at 17,000 ×g for 5 min before 500 µl of the supernatant were diluted in 500 µl of 0.014 M $H_2SO_4$. The centrifugation was repeated, and the supernatant was analyzed via Acquity UPLC BEH (WATERS) with a reversed-phase C18 column (Eurosphere II, 100 by 2.1 mm, Knauer). The separation was performed using increasing concentrations of acetonitrile in 0.1% formic acid. Commercially available crotonic acid was used as a standard in parallel with a conversion ratio of 0.893 (Koch et al., 2019).

## Non-targeted Metabolome Profiling Analysis by Gas Chromatography-Mass Spectrometry (GC-MS)

The metabolome profiling of the metabolite fraction enriched with primary metabolites was performed as previously described (Kopka et al., 2017). Twenty milliliter of the cultures were sampled by fast filtration onto 47 mm diameter glass microfiber filters of a 1.2 µm pore size (GE Healthcare, Little Chalfont, England), followed by immediate shock freezing. The complete process was < 30 s. Samples equivalent to ∼20 ml of $OD_{750}$ = 0.7–1.0 cultures were extracted for 15 min at 37°C by 1 ml methanol:chloroform:diethylamine 2.5:1.0:1.0 (v/v/v). The extraction mixture contained 0.02 mgml⁻¹ ¹³C₆-sorbitol, which was used as an internal standard (Erban et al., 2020). A polar liquid phase was obtained by adding 400 µl distilled water and centrifuging for 5 min at 14,000 rpm in an Eppendorf 5,417

microcentrifuge. The top liquid phase, ∼700 µl, was dried by vacuum centrifugation overnight in 1.5-mL microcentrifugation tubes and stored at −20°C.

The chemical derivatization for the GC analysis, GC–MS-based metabolite profiling and retention index standardization were performed as described by Erban et al. (2020) using electron impact ionization time-of-flight mass spectrometry (GC/EI-TOF–MS). The GC/EI-TOF–MS system was an Agilent 6890N24 (Agilent Technologies, Waldbronn, Germany) gas chromatograph hyphenated to a LECO Pegasus III time-of-flight mass spectrometer (LECO Instrumente GmbH, Mönchengladbach, Germany). The chromatograms were acquired, and the baseline was corrected by ChromaTOF software (LECO Instrumente GmbH, Mönchengladbach, Germany). The metabolites were annotated by manual supervision using TagFinder software (Luedemann et al., 2008), NIST2017 version 2.3[1] and the mass spectral and retention time index (RI) reference data of the Golm Metabolome Database (Kopka et al., 2005). GC/EI-TOF–MS was normalized to the internal standard ¹³C₆-sorbitol, $OD_{750}$ of the culture and volume of the sample.

## Targeted Metabolome Analysis by Liquid Chromatography-Mass Spectrometry (LC-MS)

The sampling of the cells was performed precisely as described in the previous paragraph. Low molecular mass compounds were extracted from the cells with 2 ml of ethanol (80%, HPLC grade, Roth, Germany) at 65°C for 2 h. One microgram of carnitine was added to each sample as an internal standard to correct for losses during the extraction and sample preparation. After centrifugation, the supernatants were collected and freeze-dried. The dry extracts were dissolved in 1 ml MS-grade water and filtered through 0.2 µm filters (Omnifix®-F, Braun, Germany). The cleared supernatants were analyzed using a high-performance liquid chromatograph mass spectrometer system (LCMS-8050, Shimadzu, Japan). In brief, 1 µl of each extract was separated on a pentafluorophenylpropyl (PFPP) column (Supelco Discovery HS FS, 3 µm, 150 × 2.1 mm) with a mobile phase containing 0.1% formic acid. The compounds were eluted at a rate of 0.25 ml min-1 using the following gradient: 1 min 0.1% formic acid, 95% distilled water, 5% acetonitrile, within 15 min linear gradient to 0.1% formic acid, 5% distilled water, 95% acetonitrile, 10 min 0.1% formic acid, 5% distilled water, and 95% acetonitrile. Aliquots were continuously injected into the MS/MS part and ionized via electrospray ionization (ESI). The compounds were identified and quantified using the multiple reaction monitoring (MRM) values given in the LC-MS/MS method package and the LabSolutions software package (Shimadzu, Japan). Defined standard mixes of amino acids and organic acids (usually 1 ng of the specific metabolite was injected) were analyzed in the same run to calculate the absolute contents per sample. Then, the metabolite levels were normalized to

---

[1] Available online at: http://chemdata.nist.gov/.

the detected amount of the internal standard carnitine, sample volume and $OD_{750}$.

## NAD(P) and NAD(P)H Analyses

NAD(P) and NAD(P)H were extracted from ∼8 ml of $OD_{750}$ = 0.7–1.0 cultures sampled onto 47 mm diameter glass microfiber filters of a 1.2 µm pore size (GE Healthcare, Little Chalfont, England), followed by immediate shock freezing. The quantification of NAD, NADP and NADPH was performed as previously described using enzymatic cycling assays (Zhang et al., 2020). The samples used for the NAD and NADP analyses were extracted by 500 µL extraction solution containing 0.1 M $HClO_4$ in 50% ethanol; the NADPH extraction was performed by 0.1 M KOH in 50% ethanol (Tamoi et al., 2005). The samples were thoroughly vortexed with intermittent sonication in an ice bath 3 times for 45 s each, followed by a final incubation on ice for 10 min. After centrifugation for 10 min at 14,000 rpm at 4°C, 100 µL of extract were transferred to a microcentrifuge vial and heat inactivated at 95°C for 2 min. Then, the samples were cooled on ice and neutralized either by 100 µL of 0.1 M KOH in 0.2 M Tris HCl pH 8.4 for the NAD and NADP quantitation or 100 µL of 0.1 $HClO_4$ in 0.2 M Tris HCl pH 8.4 for the NADPH analyses. The quantitation was performed using 25 or 40 µL volumes of the neutralized extracts used for the previously described cycling assays (Zhang et al., 2020). Care was taken to adjust the samples and quantitative calibration standards to identical final ethanol concentrations (**Supplementary Table 3**). In this study, the quantities of NAD, NADP and NADPH in the biological samples were sufficient for the quantitation. NADH quantitation was attempted but failed due to low concentrations in the biological samples. The analyses were biologically replicated using 3 independent cultures. The cultures were probed by 1 (NADPH) or 2 (NAD and NADP) analytical repeats, i.e., parallel samplings from the same culture. The quantitative data of the analytical repeats were averaged prior to the statistical analysis of the 3 independent biological replications.

## Metabolomic Data Analysis

All metabolomics data analyses, the hierarchical cluster analysis (HCA) by Pearson's correlation and average linkage, the principal component analysis (PCA), the two factorial analyses of variance (ANOVA), the statistical testing, e.g., Tukey tests, and the data visualization, were performed using RStudio statistical programming[2] and the program packages "impute," "multcompView," "ggplot2," "eulerr," and "https://github.com/MSeidelFed/RandodiStats_package.git." The bootstrapping analysis of the HCA tree was performed using the "pvclust" R package, and the node confidence was evaluated by "approximately unbiased" and "ordinary" bootstrap probabilities.

The relative quantification data from the GC-MS profiling analyses and quantitative data from the LC-MS analyses were maximum scaled per metabolite prior to further analyses. For the global data analyses, the missing values in the data set were replaced by the k-nearest neighbors algorithm (k-NN) and

---

[2] Available online at: https://rstudio.com/.

autoscaled. For the statistical data analyses, the data matrices were $log_{10}$-transformed after the missing data replacement by a small value, i.e., $10^{-9}$. The statistical analyses were performed using the log-transformed data. The relative concentration changes are reported as fold changes (FCs). The FCs of the metabolites that were detectable under one condition and undetectable under the compared condition, e.g., FCs comparing L to D responses or FCs comparing mutant to wild type (**Supplementary Tables 1, 2**), are reported. The significance analyses were replaced by presence and absence calls, and the FCs were scored as either significant increases or decreases.
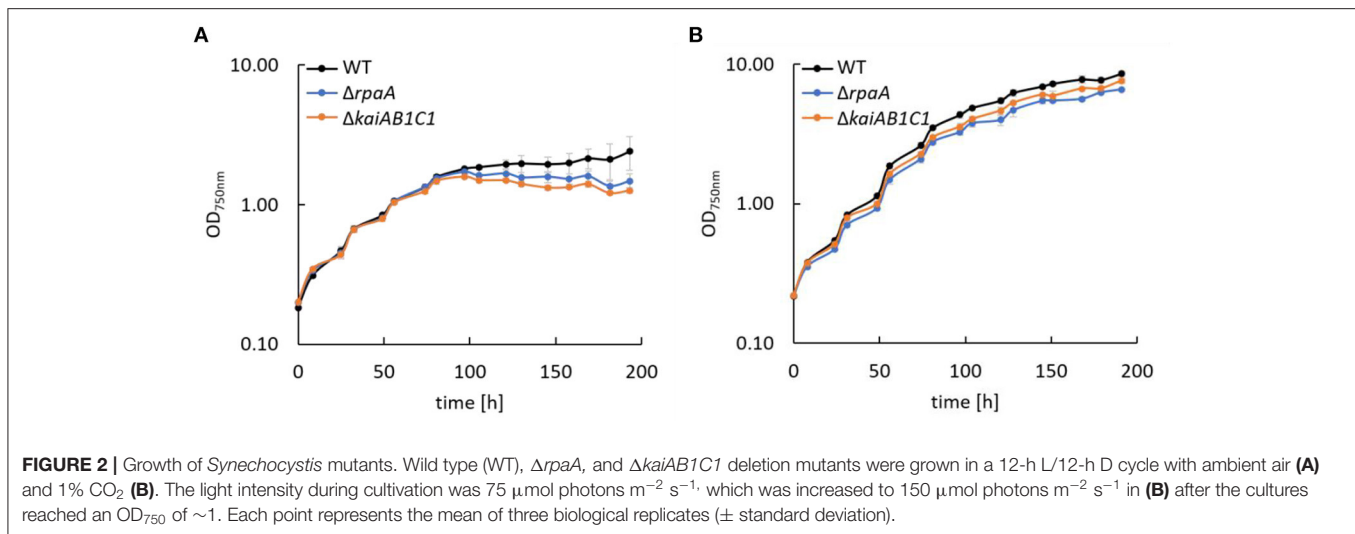
For the analyses comparing the data to previous studies, the data were merged according to the technology platform, namely, GC-MS profiling and LC-MS quantification. Merging across technology platforms was only performed if data from the same technology platform were not available. The replicate data were averaged per study maximum-scaled, and the missing values were replaced by the k-NN method. The final data matrices were log transformed and autoscaled prior to the subsequent PCA.

## RESULTS

### $CO_2$ Availability Can Compensate for the Growth Defects of Δ*kaiAB1C1* and Δ*rpaA* Mutants in L/D Cycles

Previous analyses revealed the essential role of the clock homologs KaiAB1C1 and RpaA in the viability of *Synechocystis* in L/D cycles and in the D under heterotrophic conditions (Dörrich et al., 2014; Köbler et al., 2018). Although the phenotypes of the corresponding mutants were very similar, microarray analyses revealed substantial differences in gene expression between these strains, such as an accelerated $C_i$ response that was detected only in the Δ*rpaA* mutant (Köbler et al., 2018). To determine whether $C_i$-responsive genes are still upregulated in Δ*rpaA* even under high $CO_2$ conditions, we analyzed the expression of *sbtA*, which encodes a sodium-dependent bicarbonate transporter. Using Northern blot analysis, we did not detect a difference in the *sbtA* mRNA levels between the wild-type and mutant strains under elevated $CO_2$ concentrations, suggesting that $C_i$-responsive genes are not a direct target of the RpaA transcription factor (**Supplementary Figure 1**). Furthermore, we examined the response of the mutant strains to $CO_2$ availability by growing cells under low (ambient) and high $CO_2$ (1%) conditions in liquid cultures (**Figure 2**). Similar to previous studies in which viability assays were performed using agar plates, the Δ*kaiAB1C1* and Δ*rpaA* strains showed a pronounced growth defect in L/D cycles (**Figure 2A**). The curves also revealed that growth arrest mainly appeared when the mutant cultures left the exponential growth phase (**Figure 2A**). As an organic carbon source, glucose had an additional inhibitory effect on the viability of the mutant cells (Dörrich et al., 2014; Köbler et al., 2018), whereas an increase in $CO_2$ availability could largely align the growth of the mutant cultures with the wild-type cultures in an L/D cycle (**Figure 2B**). Our previous viability analyses under mixotrophic/heterotrophic conditions and the growth assays under elevated $CO_2$ availability in this study indicate that defects in the *Synechocystis* Kai system

**FIGURE 2 |** Growth of *Synechocystis* mutants. Wild type (WT), $\Delta rpaA$, and $\Delta kaiAB1C1$ deletion mutants were grown in a 12-h L/12-h D cycle with ambient air **(A)** and 1% $CO_2$ **(B)**. The light intensity during cultivation was 75 $\mu$mol photons m$^{-2}$ s$^{-1}$, which was increased to 150 $\mu$mol photons m$^{-2}$ s$^{-1}$ in **(B)** after the cultures reached an OD$_{750}$ of ~1. Each point represents the mean of three biological replicates ($\pm$ standard deviation).

led to an imbalance in carbon acquisition and changes in central carbon metabolism.

## PHB Accumulation Is Reduced in *Synechocystis* 6803 $\Delta kaiAB1C1$ and $\Delta rpaA$ Mutants
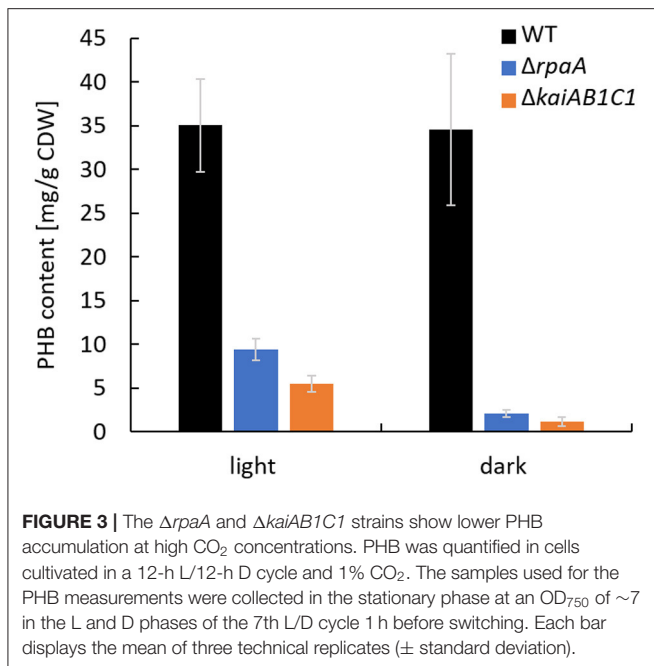
In addition to the altered $C_i$ acclimation response, the expression of two genes encoding PHB synthase subunits (*phaC* and *phaE*) was highly decreased in the $\Delta rpaA$ strain in D (Köbler et al., 2018). A similar tendency in *phaCE* transcript accumulation was also detected in a microarray analysis of the $\Delta kaiAB1C1$ strain; this tendency was less pronounced and did not match our significance criteria (Dörrich et al., 2014). In the previous microarray analyses, the cells were collected during the exponential growth phase and were grown under low $CO_2$ conditions, where PHB synthesis is very low, and the amount of this storage compound was not measurable. Therefore, we evaluated the impact of KaiAB1C1 and RpaA on PHB production under high $CO_2$ conditions during the stationary growth phase. Under these conditions, the $\Delta kaiAB1C1$ and $\Delta rpaA$ strains did not show growth arrest in an L/D cycle and exhibited only a slightly lower growth rate than the wild type (**Figure 2B**). Consistent with the lowered *pha* gene expression, both strains showed a strong reduction in PHB accumulation in the D and L phases, suggesting that the high $CO_2$ availability was unable to compensate for the defect in PHB production (**Figure 3**). Cyanobacteria produce PHB mainly under nutrient limitation. Furthermore, growth in L/D cycles increases PHB accumulation in comparison to cultivation under continuous illumination (Panda et al., 2006; Koch et al., 2020a). This indicates a diurnal regulation of PHB synthesis and a role of the D phase for its accumulation. Though the physiological role of PHB is still largely unclear, recent studies suggest a function of PHB as an electron sink during unbalanced conditions and as an additional carbon storage to prevent a metabolic spillover (Koch and Forchhammer, 2021). This complex relationship links PHB synthesis and utilization to central metabolic pathways (Ciebiada

et al., 2020; Koch et al., 2020b). Therefore, the transcriptomic changes might not fully represent the effects of KaiAB1C1 and RpaA deficiency for cellular night- and daytime functions, which led us to analyze the metabolic changes in the two corresponding mutants.

## Global Metabolic Analysis of the $\Delta rpaA$ and $\Delta kaiAB1C1$ Mutants After L/D Entrainment

The previous investigations and data presented above suggest that the KaiAB1C1 proteins along with the RpaA regulator impact primary metabolism in *Synechocystis* and growth specifically under low $C_i$ conditions in an L/D cycle (**Figure 2A**). Therefore, the metabolome of the two mutants was analyzed after an L-to-D transition under ambient $CO_2$ supply. Independent, exponentially grown precultures in ambient air were adjusted to similar optical densities of ~0.6 and sampled either in the middle of the first D phase at 5.5 h of the diurnal cycle or in the middle of the following L phase at 17.5 h (**Figure 4A**). The mutants and wild type exhibited similar growth rates during this precultivation under continuous L (**Supplementary Figure 2**). The time points were selected to avoid the expected rapid changes in metabolism directly after illumination shifts (Werner et al., 2019), to minimize the secondary effects of the growth arrest of the mutants in L/D cycles and to correlate the metabolic data of this study to previously reported transcriptomic data (Dörrich et al., 2014; Köbler et al., 2018) and to metabolic data published for *Synechococcus elongatus* PCC 7942 (Diamond et al., 2017).

We analyzed 80 metabolites from central metabolism by relative quantification of a metabolite fraction enriched for primary metabolites via gas chromatography-mass spectrometry (GC-MS)-based profiling or absolute quantification via LC-MS (**Supplementary Table 1**). In addition to the identified metabolite information, the non-targeted metabolite profiling yielded a set of yet unidentified metabolites and mass features that contributed to the global analyses of the metabolic phenotypes in this study. The hierarchical cluster and principal component

**FIGURE 3 |** The $\Delta rpaA$ and $\Delta kaiAB1C1$ strains show lower PHB accumulation at high $CO_2$ concentrations. PHB was quantified in cells cultivated in a 12-h L/12-h D cycle and 1% $CO_2$. The samples used for the PHB measurements were collected in the stationary phase at an $OD_{750}$ of ~7 in the L and D phases of the 7th L/D cycle 1 h before switching. Each bar displays the mean of three technical replicates (± standard deviation).

analyses (PCA) indicated that the switch between D and L was the major experimental factor affecting the metabolite phenotypes (**Figure 4B**) with a contribution of 31.3% to the total variance according to PC1 (**Figure 4C**, **Supplementary Figure 3**). The wild type and two mutants clustered with high bootstrapping confidence of their independent replicate profiles (**Figure 4B**). The metabolic profiles of the $\Delta kaiAB1C1$ and $\Delta rpaA$ mutants differed from those of the wild type in the D and L phases (**Figures 4B,C**). However, the metabolic phenotype of the $\Delta rpaA$ mutant differed more, especially in D, when the deviations were stronger and amounted to a distinct PC3. PC3 differentiated $\Delta rpaA$ D metabolism from all other sample profiles by 11.2% of the total variance (**Figure 4C**). The D metabolism of $\Delta rpaA$ appeared to be between that of the wild type D and L states (**Figure 4C**) with a tendency toward wild type in L (**Figure 4B**).

Molecular studies have suggested that the $\Delta rpaA$ mutant of *Synechococcus elongatus* PCC 7942 may be arrested in a dawn-like expression state (Markson et al., 2013). In wild-type *Synechocystis* cells, a set of metabolites accumulates rapidly following the onset of illumination after dawn and declines in the course of the L phase, which may indicate a morning state of metabolism (Werner et al., 2019). These "morning metabolites" include malate, fumarate, amino acids, serine, valine, isoleucine, glutamine, aspartate, arginine, and nucleotide-related metabolites, such as cytidine, cytidine monophosphate (CMP), cytidine triphosphate (CTP), uridine monophosphate (UMP), guanosine monophosphate (GMP), guanosine triphosphate (GTP), hypoxanthine, inosine, and inosine monophosphate (IMP) (Werner et al., 2019). Although our study investigated the metabolome in the middle of the L phase, two "morning metabolites," namely, aspartate and serine, significantly accumulated (Tukey test, $P < 0.05$) in the



**FIGURE 4 |** Global analysis of the metabolic L/D switch in the $\Delta kaiAB1C1$ and $\Delta rpaA$ mutants. **(A)** Design of the two-factorial entrainment experiment. Wild-type and mutant cells, i.e., the first experimental factor (genotype), were precultivated under continuous light, divided into independent cultures of $OD_{750} = 0.6$ in ambient air, and sampled in the middle of the first 12-h D phase and first 12- h L phase after entrainment, i.e., the second experimental factor (illumination). Three independent replicate cultures in each phase were analyzed by a quantitative targeted LC-MS analysis and non-targeted GC-MS metabolome profiling of the primary metabolome. **(B)** Hierarchical cluster analysis (HCA) of mutant and wild-type metabolomes. Annotated LC- and GC-MS metabolite data separately maximum scaled and then combined, log-transformed, autoscaled, and clustered using Pearson's correlation distance metric and average linkage. HCA includes a scale of the node height and bootstrap-support analysis by 1,000 iterations. The values represent the "approximately unbiased" bootstrap probability, and in brackets, the conventional bootstrap probability obtained using the "pvclust" R package is shown. Values of 100 represent the highest node probability. **(C)** Principal component analysis (PCA) of the same data. PC1 and PC3 demonstrate the

*(Continued)*

illuminated Δ*rpaA* mutant of *Synechocystis*, whereas many more metabolites shifted to higher values in the wild-type cells. In contrast, isoleucine and valine significantly accumulated during D in Δ*rpaA* (**Figure 5**). For a global comparison of our metabolite profiles and a previous diurnal characterization of *Synechocystis* central metabolism (Werner et al., 2019), we aligned the 47 commonly monitored metabolites. The PCA of the combined and separately scaled data sets revealed PC1, which had a high percentage of shared total variance, i.e., 45.8%. PC1 separated the wild-type L metabolomes from the D metabolomes of the two studies in a non-linear manner (**Supplementary Figure 4**). Colinearity indicated high agreement in the L/D-induced metabolome changes between the two studies. However, PC2, which accounted for 16.8% of the total variance, rendered a more precise alignment, and a comparison of the sampled time points between the two studies is impossible. Further comparative meta-analysis was abandoned because the studies clearly used different growth conditions. For example, high peaking light intensity at 1,600 μmol photons $m^{-2}$ $s^{-1}$ and high 5% $CO_2$ were applied in a previous study (Werner et al., 2019), whereas low light of 50 μmol photons $m^{-2}$ $s^{-1}$ and ambient $CO_2$ were applied in this study.

A global correlation analysis of the metabolites was performed using all mutant and wild-type data in the current study. We present this analysis as a Pearson's correlation matrix that analyzes the relative concentration changes in all monitored metabolites (**Supplementary Figure 5**). This analysis indicates a central group of highly correlated metabolites that contained metabolites of lower glycolysis, 3-phosphoglycerate (3PGA), 2-phosphoglycerate (2PGA), phosphoenolpyruvate (PEP), and of photorespiration, 2-phosphoglycolate (2PG), serine and glycerate. Two additional large groups contained metabolites that were inversely correlated between the groups but partially formed highly correlated subsets within each group. The first group comprised most amino acids and the oxidative (C6-C5) branch of tricarboxylic acid (TCA) metabolism. The second group contained predominantly metabolites of nucleic acid metabolism and the reductive (C4) branch of TCA metabolism (**Supplementary Figure 5**).

## Δ*kaiAB1C1* and Δ*rpaA* Mutations Attenuate Metabolic L/D Responses

Our study revealed that 46 metabolites, i.e., more than half of all monitored compounds, significantly (Tukey test, $P < 0.05$) differed between the mutants and wild type. A large overlap of 21 metabolic changes during the L/D cycle was observed between the two mutants (**Figure 6**). This finding

supported the hypothesis that the KaiAB1C1 system contributes to the diurnal control of central metabolism mostly via RpaA-mediated output signaling (**Figure 1**). Most of the common metabolic defects were apparent in both phases (12), except for one defect, which was limited to the L phase (9). Deviations specific to only one mutant suggested a small RpaA-independent metabolic signaling component in the KaiAB1C1 system, with three metabolic changes in D, one metabolic change in L and one metabolic change in both. In contrast, the KaiAB1C1-independent changes in the Δ*rpaA* mutant (20) exhibited a preference for RpaA-specific metabolic defects in D (10) (**Figure 6**), which is consistent with the closer clustering of Δ*rpaA* D with the L samples of all strains (see **Figure 4**). The larger impact of the RpaA deficiency may be explained by its functionality as a transcription factor with partly retained functions in the absence of Kai-based control and the KaiAB1C1-independent additional functions of RpaA that are established via protein-protein interactions (Köbler et al., 2018). For example, RpaA interacts with RpaB, which is the transcriptional regulator responding to environmental changes, including L/D transitions, via concomitant redox regulation (Riediger et al., 2019) (**Figure 1**).

The set of 46 mutant-dependent metabolites included unidentified compounds and metabolites with small but significant pool size changes (**Supplementary Table 1**). To focus our data analysis, for the following analysis, we selected only identified metabolites that were significantly (Tukey test, $P \leq 0.05$) responsive to the L/D change (**Figure 5**). From this subset, we distinguished five groups of L/D-responsive metabolites (L/D groups) according to their relative changes in the wild type compared to the mutant defects. L/D group I contained 17 metabolites (mostly amino acids) that accumulated in the wild type in L compared to D (**Figure 5**). A second set of 11 metabolites, i.e., L/D group II, exhibited inverse changes in the wild type compared to group I and contained metabolites, e.g., organic acids, that decreased in L compared to D. Only a small set of metabolites from these two groups, namely, arginine, aspartate, proline (L/D group I) and malate (L/D group II), maintained L/D responsiveness in the mutants. KaiAB1C1 and especially the RpaA deficiency attenuated the L/D responsiveness of a large fraction of L/D-responsive metabolites in both groups. Many attenuated changes were shared between the Δ*rpaA* and Δ*kaiAB1C1* mutants. However, the Δ*rpaA* mutant clearly had more metabolites with attenuated L/D responsiveness (**Figure 5**).

Furthermore, we discovered additional but rarer metabolite response patterns supporting the hypothesis that central metabolic responses to a switch between photoautotrophy and D-induced heterotrophy are all but passive. These metabolic responses are enhanced and modulated by KaiAB1C1 and/or RpaA. Glutamate (L/D group III) represented one of these rarer patterns as it accumulated in the wild type in the L phase and had an inverted L/D response only in the Δ*rpaA* mutant. Similarly, pyruvate and histidine (L/D group IV) were depleted in the wild type in the L and accumulated in the Δ*rpaA* mutant (**Figure 5**). Some metabolites (L/D-group V), e.g., N-acetyl-glutamate, glutamine, ornithine-1,5-lactam, lysine, citrate/isocitrate, TMP and CMP, even gained significant L/D
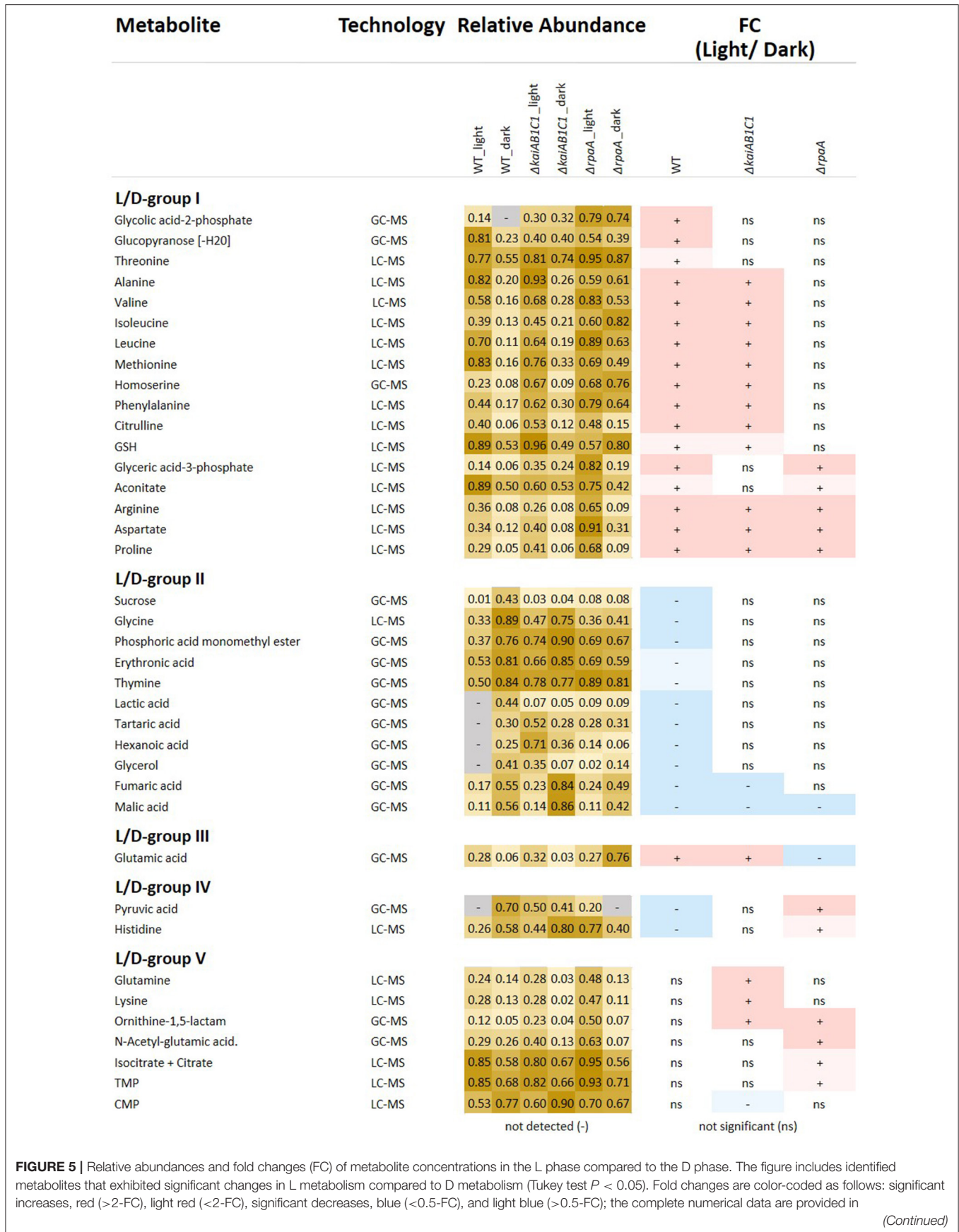
| Metabolite | Technology | Relative Abundance | | | | | | FC (Light/ Dark) | | |
|---|---|---|---|---|---|---|---|---|---|---|
| | | WT_light | WT_dark | ΔkaiAB1C1_light | ΔkaiAB1C1_dark | ΔrpaA_light | ΔrpaA_dark | WT | ΔkaiAB1C1 | ΔrpaA |
| **L/D-group I** | | | | | | | | | | |
| Glycolic acid-2-phosphate | GC-MS | 0.14 | - | 0.30 | 0.32 | 0.79 | 0.74 | + | ns | ns |
| Glucopyranose [-H20] | GC-MS | 0.81 | 0.23 | 0.40 | 0.40 | 0.54 | 0.39 | + | ns | ns |
| Threonine | LC-MS | 0.77 | 0.55 | 0.81 | 0.74 | 0.95 | 0.87 | + | ns | ns |
| Alanine | LC-MS | 0.82 | 0.20 | 0.93 | 0.26 | 0.59 | 0.61 | + | + | ns |
| Valine | LC-MS | 0.58 | 0.16 | 0.68 | 0.28 | 0.83 | 0.53 | + | + | ns |
| Isoleucine | LC-MS | 0.39 | 0.13 | 0.45 | 0.21 | 0.60 | 0.82 | + | + | ns |
| Leucine | LC-MS | 0.70 | 0.11 | 0.64 | 0.19 | 0.89 | 0.63 | + | + | ns |
| Methionine | LC-MS | 0.83 | 0.16 | 0.76 | 0.33 | 0.69 | 0.49 | + | + | ns |
| Homoserine | GC-MS | 0.23 | 0.08 | 0.67 | 0.09 | 0.68 | 0.76 | + | + | ns |
| Phenylalanine | LC-MS | 0.44 | 0.17 | 0.62 | 0.30 | 0.79 | 0.64 | + | + | ns |
| Citrulline | LC-MS | 0.40 | 0.06 | 0.53 | 0.12 | 0.48 | 0.15 | + | + | ns |
| GSH | LC-MS | 0.89 | 0.53 | 0.96 | 0.49 | 0.57 | 0.80 | + | + | ns |
| Glyceric acid-3-phosphate | LC-MS | 0.14 | 0.06 | 0.35 | 0.24 | 0.82 | 0.19 | + | ns | + |
| Aconitate | LC-MS | 0.89 | 0.50 | 0.60 | 0.53 | 0.75 | 0.42 | + | ns | + |
| Arginine | LC-MS | 0.36 | 0.08 | 0.26 | 0.08 | 0.65 | 0.09 | + | + | + |
| Aspartate | LC-MS | 0.34 | 0.12 | 0.40 | 0.08 | 0.91 | 0.31 | + | + | + |
| Proline | LC-MS | 0.29 | 0.05 | 0.41 | 0.06 | 0.68 | 0.09 | + | + | + |
| **L/D-group II** | | | | | | | | | | |
| Sucrose | GC-MS | 0.01 | 0.43 | 0.03 | 0.04 | 0.08 | 0.08 | - | ns | ns |
| Glycine | LC-MS | 0.33 | 0.89 | 0.47 | 0.75 | 0.36 | 0.41 | - | ns | ns |
| Phosphoric acid monomethyl ester | GC-MS | 0.37 | 0.76 | 0.74 | 0.90 | 0.69 | 0.67 | - | ns | ns |
| Erythronic acid | GC-MS | 0.53 | 0.81 | 0.66 | 0.85 | 0.69 | 0.59 | - | ns | ns |
| Thymine | GC-MS | 0.50 | 0.84 | 0.78 | 0.77 | 0.89 | 0.81 | - | ns | ns |
| Lactic acid | GC-MS | - | 0.44 | 0.07 | 0.05 | 0.09 | 0.09 | - | ns | ns |
| Tartaric acid | GC-MS | - | 0.30 | 0.52 | 0.28 | 0.28 | 0.31 | - | ns | ns |
| Hexanoic acid | GC-MS | - | 0.25 | 0.71 | 0.36 | 0.14 | 0.06 | - | ns | ns |
| Glycerol | GC-MS | - | 0.41 | 0.35 | 0.07 | 0.02 | 0.14 | - | ns | ns |
| Fumaric acid | GC-MS | 0.17 | 0.55 | 0.23 | 0.84 | 0.24 | 0.49 | - | - | ns |
| Malic acid | GC-MS | 0.11 | 0.56 | 0.14 | 0.86 | 0.11 | 0.42 | - | - | - |
| **L/D-group III** | | | | | | | | | | |
| Glutamic acid | GC-MS | 0.28 | 0.06 | 0.32 | 0.03 | 0.27 | 0.76 | + | + | - |
| **L/D-group IV** | | | | | | | | | | |
| Pyruvic acid | GC-MS | - | 0.70 | 0.50 | 0.41 | 0.20 | - | - | ns | + |
| Histidine | LC-MS | 0.26 | 0.58 | 0.44 | 0.80 | 0.77 | 0.40 | - | ns | + |
| **L/D-group V** | | | | | | | | | | |
| Glutamine | LC-MS | 0.24 | 0.14 | 0.28 | 0.03 | 0.48 | 0.13 | ns | + | ns |
| Lysine | LC-MS | 0.28 | 0.13 | 0.28 | 0.02 | 0.47 | 0.11 | ns | + | ns |
| Ornithine-1,5-lactam | GC-MS | 0.12 | 0.05 | 0.23 | 0.04 | 0.50 | 0.07 | ns | + | + |
| N-Acetyl-glutamic acid. | GC-MS | 0.29 | 0.26 | 0.40 | 0.13 | 0.63 | 0.07 | ns | ns | + |
| Isocitrate + Citrate | LC-MS | 0.85 | 0.58 | 0.80 | 0.67 | 0.95 | 0.56 | ns | ns | + |
| TMP | LC-MS | 0.85 | 0.68 | 0.82 | 0.66 | 0.93 | 0.71 | ns | ns | + |
| CMP | LC-MS | 0.53 | 0.77 | 0.60 | 0.90 | 0.70 | 0.67 | ns | - | ns |

not detected (-)                    not significant (ns)

**FIGURE 5 |** Relative abundances and fold changes (FC) of metabolite concentrations in the L phase compared to the D phase. The figure includes identified metabolites that exhibited significant changes in L metabolism compared to D metabolism (Tukey test $P < 0.05$). Fold changes are color-coded as follows: significant increases, red (>2-FC), light red (<2-FC), significant decreases, blue (<0.5-FC), and light blue (>0.5-FC); the complete numerical data are provided in
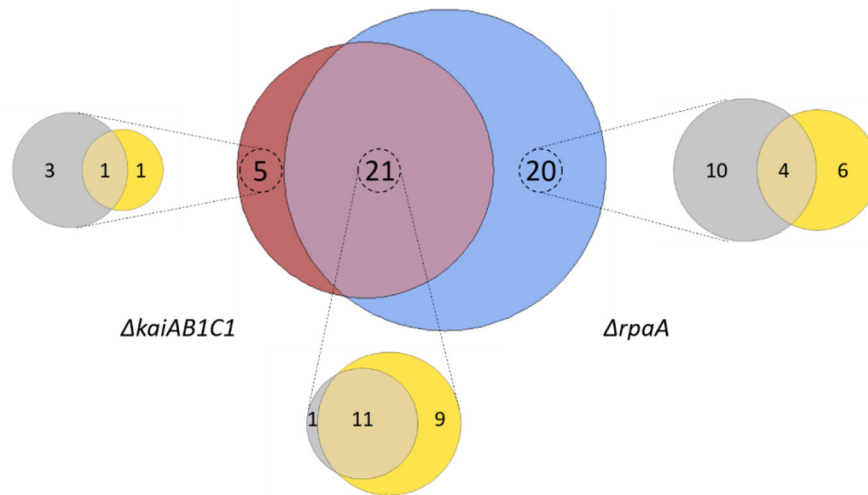
*(Continued)*

**FIGURE 6 |** Summary of the metabolic changes in the mutants of *Synechocystis*. Venn diagram analysis of all significant (Tukey test, $P < 0.05$) metabolic changes among the set of identified and yet unidentified metabolites. Intersections show significant changes in the metabolite pools shared between the Δ*kaiAB1C1* (brown) and Δ*rpaA* (blue) mutants. Zoom-ins show the contribution of the two diurnal phases to the respective sets, D phase (gray) and L phase (yellow). Note the large overlap between the mutants and the more frequent specific responses of the Δ*rpaA* cells.

responsiveness in one or both mutants (**Figure 5**). Further central metabolites, e.g., 2PGA and PEP, exhibited response patterns similar to those of L/D group IV but had only small effect sizes and failed to pass the significance threshold (**Supplementary Table 1**).

## Δ*kaiAB1C1* and Δ*rpaA* Mutations Affect Central Metabolic Pathways

The preceding part of our metabolic analysis highlighted only one factor of our two-factorial study, namely, the change in illumination and the respective photoautotrophy to heterotrophy transitions of metabolism. However, the attenuation of the L/D response ratios compared to those of the wild type can have multiple alternative causes. Among other causes, the loss of L/D responsiveness can be explained by a deficiency to accumulate a metabolite pool that should increase upon illumination or a failure to decrease metabolites upon D transition that are high in L. The latter explanation applied in the analysis of the Δ*rpaA* mutant to a large set of metabolites from L/D-group I (**Figure 5**, relative-abundance section). Specifically, a set of amino acids, including alanine and the branched chain amino acids valine, isoleucine, or leucine, retained high concentrations upon the D transition (**Figure 5**). Similarly, 2PG lost L/D responsiveness in both the Δ*rpaA* and the Δ*kaiAB1C1* mutants, but Δ*kaiAB1C1* showed a non-significant illumination-independent increase compared to the extreme and highly significant accumulation of 2PG in the Δ*rpaA* mutant (**Figure 7**). In the following section, we specifically compared the mutant defects with the wild-type (**Supplementary Table 2**), thereby focusing on pathways

that contain metabolites with large concentration changes to identify the fundamental metabolic aspects associated with the mutant defects.

### Lower Glycolysis

The two products of RubisCO, namely, the carboxylation product 3PGA and the oxygenation product 2PG, were highly elevated in the L samples of the Δ*rpaA* mutant and, to a lesser extent, in the Δ*kaiAB1C1* mutant (**Figure 7**). These increases suggested enhanced RubisCO activity. To support this hypothesis, we analyzed the amount of RubisCO in the mutants by a Western blot analysis (**Figure 8**). Compared to the wild type, the Δ*kaiAB1C1* and Δ*rpaA* cells accumulated more of the RbcL subunit in L and D, suggesting that the higher amounts of 3PGA and 2PG could indeed be based on a cellular increase in the RubisCO concentration. The higher amounts of 3PGA in the Δ*rpaA* mutant were consistently associated with lower glycolysis with accumulating 2PGA and PEP concentrations in this strain. These findings suggest an activation of carbon utilization from the CBB cycle in the direction of lower glycolysis and toward the oxidative branch of the TCA cycle in the absence of RpaA.

The assumption of the preferred use of 3PGA in the illuminated Δ*rpaA* mutant by lower glycolysis and not by gluconeogenesis was supported by the L levels of soluble carbohydrates, such as sucrose, which were not significantly changed in the Δ*rpaA* cells (**Supplementary Table 1**). Similar changes in lower glycolysis and carbohydrate metabolism occur in *Synechocystis* cells shifted from high- to low-$CO_2$-supply (Orf et al., 2015). The imbalance of carbon use in favor of
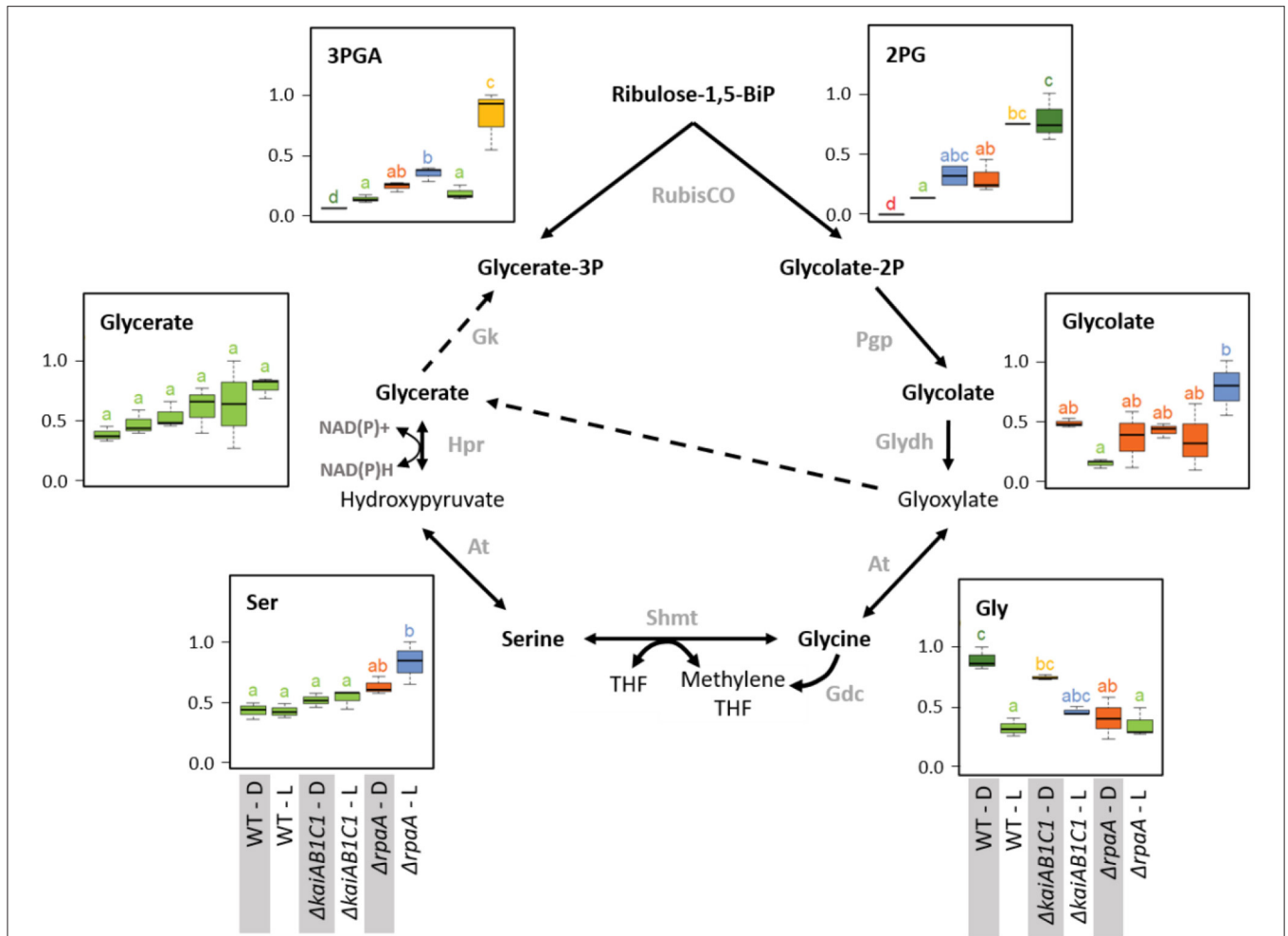
**FIGURE 7 |** Photorespiration. Box plots showing the maximum normalized relative changes in the metabolite concentrations and Tukey test results ($P < 0.05$, $n = 3$). Metabolite levels that significantly differ are indicated by lowercase letters and color coding. Note the moderate and strong increases in the RubisCO products 3PGA and 2PG in the $\Delta kaiAB1C1$ mutant and the $\Delta rpaA$ mutant, respectively. High 2PG accumulation in the $\Delta rpaA$ mutant continues in the D phase and is associated with glycolate accumulation in the L phase. Serine and glycine respond inversely to RpaA deficiency. Glycine fails to accumulate in the D, while serine accumulates in the L. Dashed arrows indicate multiple reaction steps. Relevant enzymes and complexes include (gray) glycolate-2P phosphatase (Pgp), glycolate dehydrogenase (Glydh), aminotransferase (At), glycine decarboxylase complex (Gdc), serine hydroxymethyltransferase (Shmt), tetrahydrofolate (THF), hydroxypyruvate reductase (Hpr), and glycerate kinase (Gk).
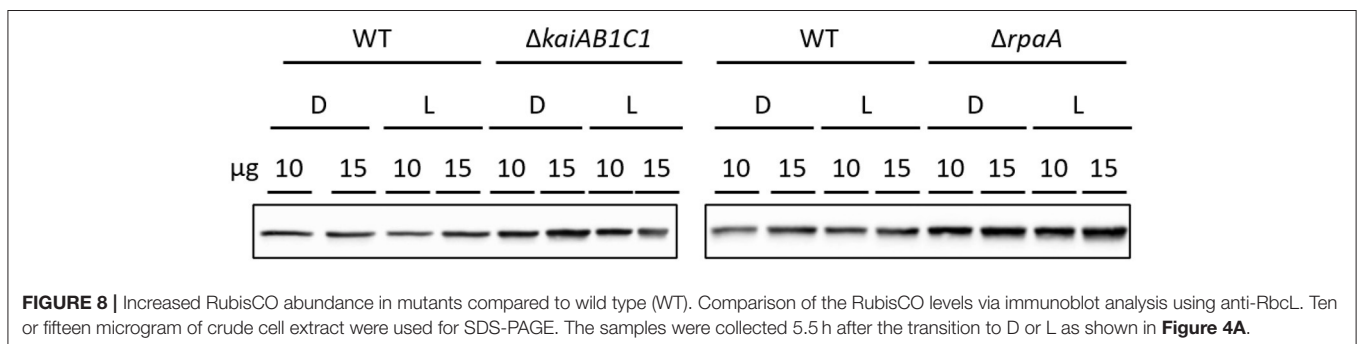


**FIGURE 8 |** Increased RubisCO abundance in mutants compared to wild type (WT). Comparison of the RubisCO levels via immunoblot analysis using anti-RbcL. Ten or fifteen microgram of crude cell extract were used for SDS-PAGE. The samples were collected 5.5 h after the transition to D or L as shown in **Figure 4A**.

lower glycolysis may be controlled via the newly discovered PII-regulated switch of phosphoglycerate mutase (PGAM) activity via PirC (Orthwein et al., 2021). Previous gene expression

studies implied that *PirC (sll0944)* is downregulated in the $\Delta rpaA$ mutant under L conditions but not in D, although these data did not meet our significance criteria (Köbler et al., 2018). Hence, the

lower PGAM inhibition in the $\Delta rpaA$ mutant likely stimulates the higher flux to 2PGA, PEP, and pyruvate compared to the wild type.

The disbalanced carbon utilization in the $\Delta rpaA$ cells extended to the pyruvate family of amino acids, i.e., alanine, and the branched chain amino acids leucine, isoleucine and valine. Hence, pyruvate is crucial for metabolism and cannot be depleted without affecting cyanobacterial growth (Kopka et al., 2017). According to its high demand during growth in the L, the pyruvate levels declined in the wild type upon transition from D to L. The pyruvate decrease was consistent with associated increases in the pyruvate amino acid family in the L (**Supplementary Table 1**). These amino acid responses remained unaltered in the $\Delta kaiAB1C1$ cells, but alanine, leucine, isoleucine and valine consistently overaccumulated in the darkened $\Delta rpaA$ cells (**Figure 9**). The deregulation of amino acid biosynthesis in the $\Delta rpaA$ mutant can contribute to the observed pyruvate depletion and may ultimately affect growth.

## Photorespiration

The previously mentioned increased amounts of photorespiratory 2PG extended within the pathway toward higher amounts of glycolate and serine but not glycine in the illuminated $\Delta rpaA$ cells (**Figure 7**). Glycine lost L/D responsiveness in the $\Delta rpaA$ cells, and the balance of the NADH-producing glycine decarboxylase complex (GDC) and serine hydroxymethyltransferase (SHMT) reaction favored serine. Photorespiratory metabolism was not significantly changed in the $\Delta kaiAB1C1$ mutant, which is consistent with the only marginal increase in 2PG in this mutant. The increased 2PG and glycolate levels indicate an increased flux into the *Synechocystis* photorespiratory pathway (Eisenhut et al., 2008; Huege et al., 2011) that detoxifies the critical substrate 2PG. The growth defect of the $\Delta rpaA$ cells in the L/D cycle is clearly associated with constitutively elevated 2PG levels. This observation is consistent with the finding that 2PG inhibits several key enzymes in plant primary carbon metabolism (e.g., Flügel et al., 2017). Furthermore, *Synechocystis* uses 2PG accumulation as a metabolic signal that activates the expression of cyanobacterial carbon-concentrating metabolism (CCM) because 2PG stimulates the activator CmpR and inactivates the repressor protein NdhR (Nishimura et al., 2008; Jiang et al., 2018). CCM components, such as *sbtB, ndhD3, ndhF3, cupA, cmpA,* and *cmpB* (Shibata et al., 2001, 2002; Xu et al., 2008; Orf et al., 2015), are consistently expressed at higher mRNA levels during the L phase in $\Delta rpaA$ cells (Köbler et al., 2018).

Consistent with the previously reported deregulation of photosystem I and phycobilisome gene expression in the D phase (Köbler et al., 2018), the 2PG levels largely remained at increased levels in the non-illuminated $\Delta rpaA$ mutant cells. In contrast, the amount of 3PGA consistently decreased in the D phase because inorganic carbon assimilation halted. RubisCO is assumed to be inactive during the night, but other sources of 2PG synthesis seem unlikely. An explanation of mistimed 2PG accumulation is proposed by the hypothesis that RubisCO may not be fully inactivated in $\Delta rpaA$ mutant cells during the 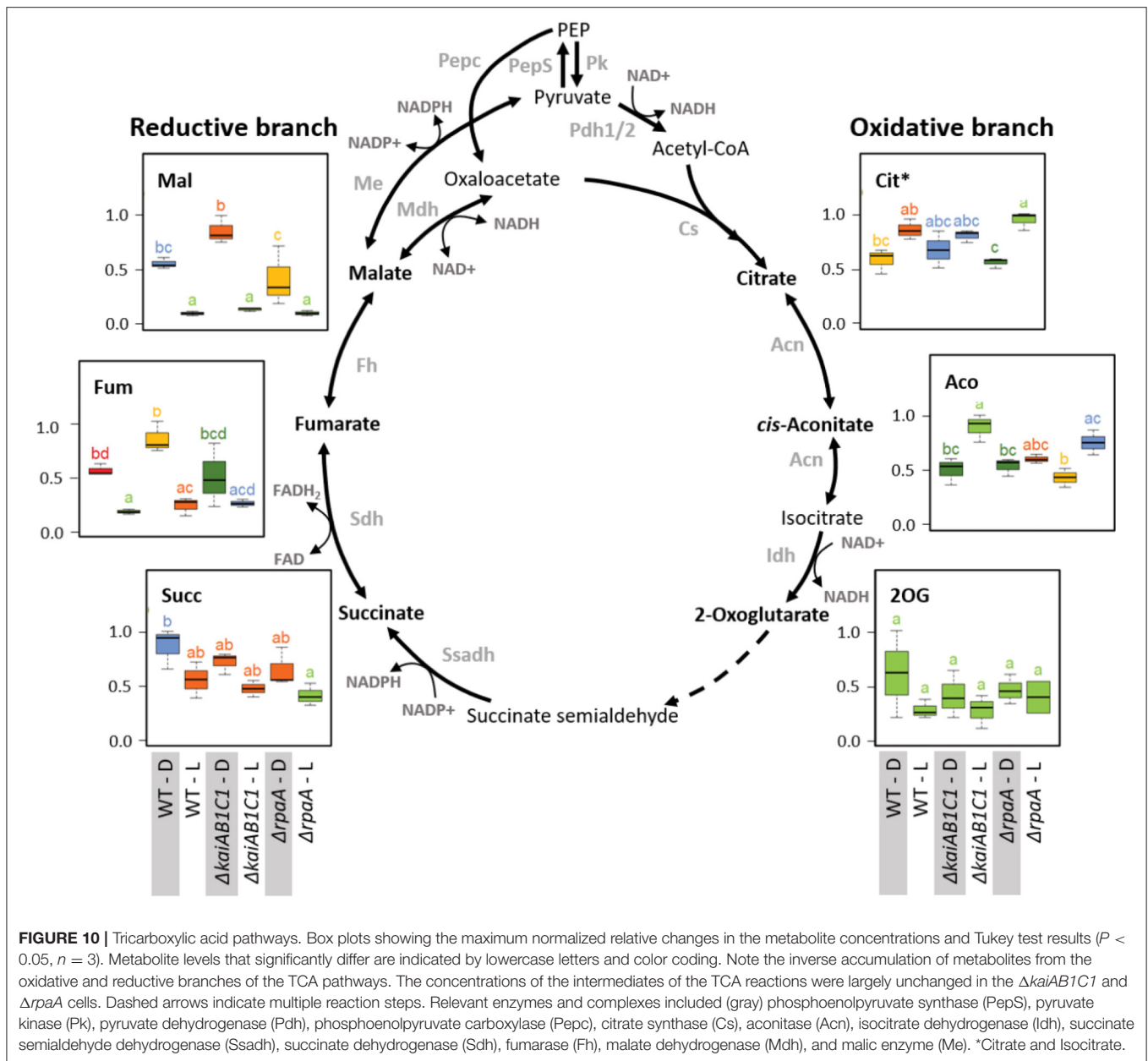D-phase, especially because there seems to be substantial overaccumulation of this enzyme in these cells (**Figure 8**). RubisCO which is not completely inactivated may then preferentially perform oxygenation during the D phase due to the low $C_i$/high $O_2$ intracellular environment. This explanation not only applies to the mutant cells but also seems to apply to the wild type, which fully detoxifies 2PG in D but still contains significantly higher amounts of glycolate and glycine in D compared to the L (**Figure 7**). An alternative explanation of elevated 2PG in D may be a potential carry-over of the high concentration from the preceding L phase. Such an assumption could imply D inhibition of the 2PG dephosphorylation step in the $\Delta rpaA$ mutant. However, regulation of the 2PG phosphatase step seems unlikely because of the presence of up to four partially highly promiscuous 2-PG phosphatases within the *Synechocystis* genome (Rai et al., 2018).

## TCA Pathways

Our metabolome analysis covered most metabolites of the non-canonical TCA cycle (**Figure 10**) and associated amino acid biosynthesis pathways that receive carbon building blocks from this cycle (**Figure 11**). Among cyanobacteria, the TCA cycle is not closed because the 2-oxoglutarate (2OG) dehydrogenase complex is missing. Two shunts have been described that can circumvent the missing 2OG dehydrogenase toward succinate, however, the flux through these shunts seem to be minor under most growth conditions (Zhang and Bryant, 2011; Xiong et al., 2014). The predominant open nature of the TCA pathways is clearly reflected in our current study by the inverted L/D responses of the TCA cycle metabolites from its reductive (C4) and oxidative (C6 and C5) branches. Malate, fumarate and succinate of the reductive branch decreased in L with large decreases in the malate and fumarate pools in all strains but only minor changes in succinate. This consistent L/D response indicates carbon utilization by respiration via the succinate dehydrogenase complex in D and the inactivation or reversion of this process in L. In contrast, the intermediates of the oxidative branch, such as citrate and aconitate, accumulated in L and reflected enhanced use of photosynthetically fixed organic carbon by ammonia assimilation via glutamine synthetase/glutamine:2-oxoglutarate aminotransferase (GS/GOGAT cycle). However, the amount of 2OG did not significantly differ between the L and D samples of all strains, ruling out the possibility that 2OG-mediated signaling was responsible for the observed expression changes in the CCM-related genes. The deficiency of the KaiAB1C1 system and the RpaA regulator did not affect the TCA pathways, but the utilization of carbon in the associated nitrogen assimilation is reported in the following section.

## Nitrogen Assimilation and Amino Acid Biosynthesis

In addition to 2OG, the products of the GS/GOGAT cycle, i.e., glutamine and glutamate, and the subsequent aminotransferase product aspartate accumulate in illuminated wild-type cells (**Figure 11**). The accumulation of these amino acids paralleled the changes in the oxidative TCA branch. These concentration changes are consistent with the operation of ammonia assimilation in the L. Nitrogen (N)-assimilation requires the products of photosynthetic light reactions,
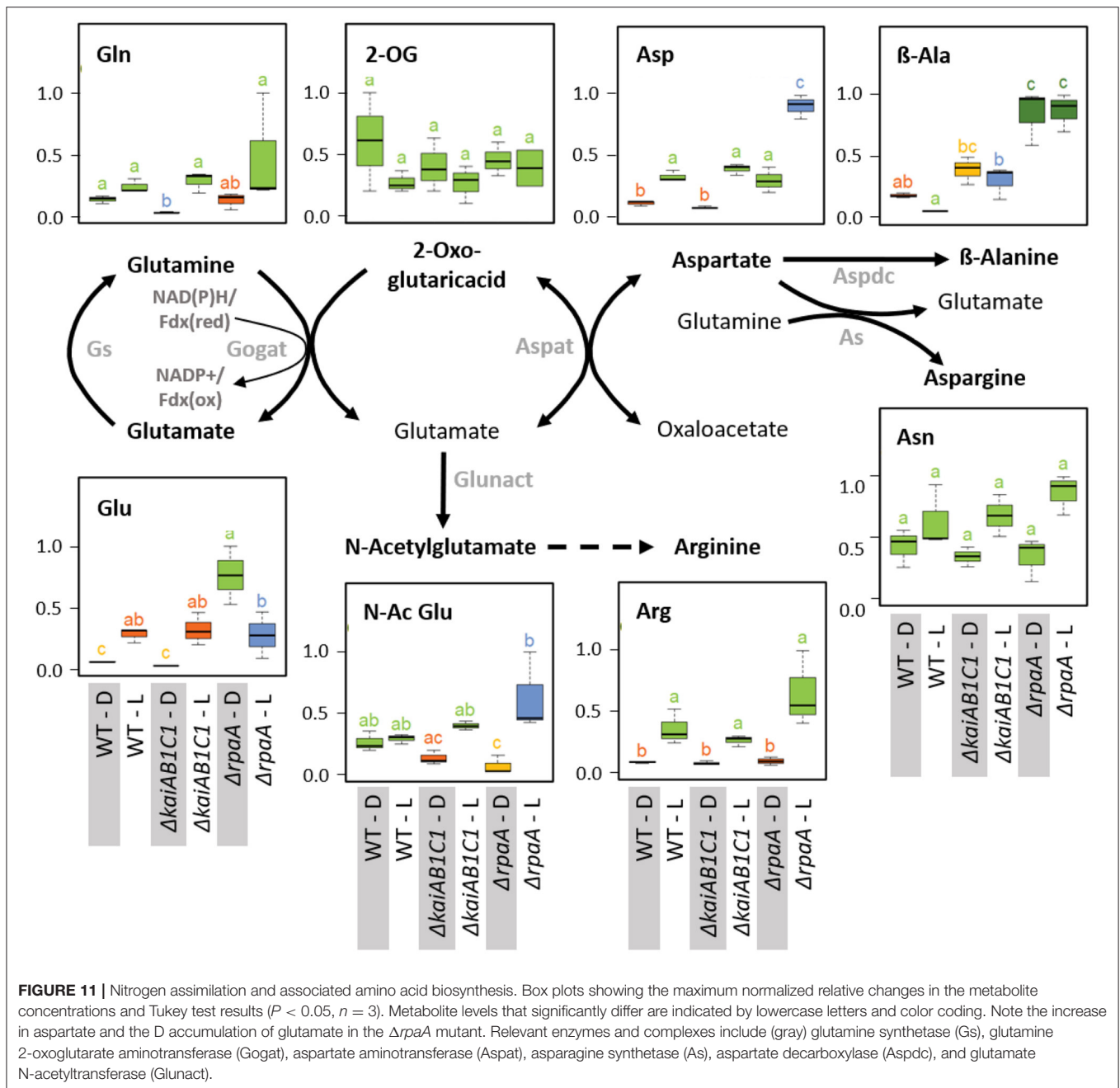
**FIGURE 9 |** Lower glycolysis, glutamate, and the pyruvate family of amino acids. Box plots showing the maximum normalized relative changes in the metabolite concentrations and Tukey test results ($P < 0.05$, $n = 3$). Metabolite levels that significantly differ are indicated by lowercase letters and color coding. Note the subtle changes in the $\Delta kaiAB1C1$ mutant, while the $\Delta rpaA$ mutant exhibited significantly increased pyruvate family amino acids, 3PGA, PEP, and glutamate in D. These changes are accompanied by pyruvate depletion in the D phase relative to the wild type. In the L, 3PGA accumulates in the $\Delta kaiAB1C1$ mutant relative to the wild type. In the $\Delta rpaA$ mutant, 3PGA accumulates to even higher levels, and the 2PGA and PEP increases become significant. Dashed arrows indicate multiple reaction steps. Relevant enzymes and complexes include (gray) ribulose-1,5-bisphosphate carboxylase-oxygenase (RubisCO), phosphoglycerate mutase (Pgam), enolase (Eno), phosphoenolpyruvate synthase (Peps), pyruvate kinase (Pk), pyruvate dehydrogenase (Pdh), alanine dehydrogenase (Aladh), and alanine transaminase (Alat).

such as ATP and reduced ferredoxin. Similar to the TCA pathways, the deficiency of KaiAB1C1 proteins did not affect ammonium assimilation or the associated glutamate/aspartate

metabolism. The $\Delta rpaA$ mutant, however, differed in the L/D responses of glutamate but not of glutamine; specifically, the glutamate concentrations increased in D (**Figure 11**). This

**FIGURE 10 |** Tricarboxylic acid pathways. Box plots showing the maximum normalized relative changes in the metabolite concentrations and Tukey test results ($P <$ 0.05, $n = 3$). Metabolite levels that significantly differ are indicated by lowercase letters and color coding. Note the inverse accumulation of metabolites from the oxidative and reductive branches of the TCA pathways. The concentrations of the intermediates of the TCA reactions were largely unchanged in the $\Delta kaiAB1C1$ and $\Delta rpaA$ cells. Dashed arrows indicate multiple reaction steps. Relevant enzymes and complexes included (gray) phosphoenolpyruvate synthase (PepS), pyruvate kinase (Pk), pyruvate dehydrogenase (Pdh), phosphoenolpyruvate carboxylase (Pepc), citrate synthase (Cs), aconitase (Acn), isocitrate dehydrogenase (Idh), succinate semialdehyde dehydrogenase (Ssadh), succinate dehydrogenase (Sdh), fumarase (Fh), malate dehydrogenase (Mdh), and malic enzyme (Me). *Citrate and Isocitrate.

increase was associated with a significant accumulation of aspartate in the D and consistent with the supply directly from glutamate via the aspartate aminotransferase reaction, while the carbon backbone, oxaloacetate, may be supplied by phosphoenolpyruvate carboxylase (PEPC), malate dehydrogenase and the intermediates of the reductive TCA branch. The lack of a concomitant accumulation of 2OG indicated active reuse by the GS/GOGAT cycle. Upon illumination, the $\Delta rpaA$ cells overaccumulated Asp and N-acetylglutamate, which is an additional direct product of glutamate in the pathway toward arginine biosynthesis (**Figure 11**). Collectively, our observations indicate overly active N assimilation in $\Delta rpaA$ cells that extends in D to multiple

proteinogenic amino acid pools (**Figure 5**). Furthermore, in both diurnal phases, the amounts of non-proteinogenic amino acids, such as β-alanine and homoserine, increased, while nucleobases, such as thymine and uracil, increased in L (**Figure 11**, **Supplementary Table 2**). We hypothesize that the $\Delta rpaA$ mutant may not stop N-assimilation during the D phase for an unknown reason.

## Metabolic Cofactors

The set of nucleotides and nucleosides monitored in the current study mostly exhibited minor pool changes that did not pass the significance threshold (**Supplementary Tables 1, 2**). The lack of significance in our study likely results from the high variation

**FIGURE 11 |** Nitrogen assimilation and associated amino acid biosynthesis. Box plots showing the maximum normalized relative changes in the metabolite concentrations and Tukey test results ($P < 0.05$, $n = 3$). Metabolite levels that significantly differ are indicated by lowercase letters and color coding. Note the increase in aspartate and the D accumulation of glutamate in the $\Delta rpaA$ mutant. Relevant enzymes and complexes include (gray) glutamine synthetase (Gs), glutamine 2-oxoglutarate aminotransferase (Gogat), aspartate aminotransferase (Aspat), asparagine synthetase (As), aspartate decarboxylase (Aspdc), and glutamate N-acetyltransferase (Glunact).

in the sampling time in the middle of the L phase. This phase still represents a time during which the concentrations of many nucleotides and nucleosides return from high levels in the morning (Saha et al., 2016) to the low levels present at the end of the day and during the night (Werner et al., 2019).

The levels of glutathione (GSH) and flavin mononucleotide (FMN) fluctuated less. Both metabolites indicate the deregulation of the redox state in $\Delta kaiAB1C1$ cells and greater deregulation in the $\Delta rpaA$ mutant. GSH failed to increase upon illumination in the $\Delta rpaA$ cells, whereas

FMN accumulated constitutively in both the $\Delta kaiAB1C1$ and $\Delta rpaA$ cells.

Motivated by these observations, we monitored the nicotinamide adenine dinucleotide redox cofactors $NADP^+$, NADPH, $NAD^+$ and NADH. $NADP^+$, NADPH and $NAD^+$ were quantified, but these nucleotides and nucleosides did not pass our significance threshold (**Supplementary Table 3**). NADH was not detectable due to low concentrations. Our measurements indicated that $NADP^+$, NADPH, $NAD^+$, and the NADPH/NADP ratio potentially increased in the wild type in the L phase compared to D. This increase in the NADPH/NADP

ratio in L appeared to be absent from the $\Delta kaiAB1C1$ and $\Delta rpaA$ mutant cells. In both mutants, this observation can be explained by an increase in the NADPH levels in the D (**Supplementary Table 3**).

## DISCUSSION

Based on metabolome analyses of *Synechocystis* mutants in L and D samples of autotrophically grown cultures, we can conclude that the *Synechocystis* KaiAB1C1-SasA-RpaA potential timing system largely affects the metabolic switch from photoautotrophy in L to the usage of internal carbon reserves in D. This effect is comparable to the function of the *Synechococcus* sp. PCC 7942 circadian clock system, although the effects of the clock deficiency on the transcriptomic and metabolomic levels differ between these two cyanobacteria. These strain-specific differences are likely caused by differential adaptation of the two cyanobacteria. Facultative heterotrophy and the presence of alternative putative clock components in *Synechocystis* inevitably impact the transcriptional regulatory network with divergent metabolic consequences in the two cyanobacterial strains. Our findings suggest that the molecular mechanisms unraveled in one model organism may differ from those in other strains due to adaptive evolution. This assumption is consistent with findings suggesting that paralog duplications may quickly vanish from cyanobacterial genomes, e.g., of *Acaryochloris* or *Chlorogloeopsis* strains, unless they provide fitness benefits (Miller et al., 2011; Weissenbach et al., 2017). This reasoning likely applies to clock oscillator-related genes; for instance, the *Nostoc linckia kaiABC* gene family has been shown to respond to long-term differential stress by rapid adaptive radiation (Dvornyk et al., 2002).

In our *Synechocystis* model, the *rpaA* deletion had a much larger effect on metabolism than the *kaiAB1C1* mutation, which is consistent with the more pronounced transcriptional changes in $\Delta rpaA$ (Köbler et al., 2018), although both mutants grew very similarly under these conditions. Most interestingly, $\Delta rpaA$ showed a remarkable overaccumulation of 2PG and amino acids in D with concurrent effects on the redox balance. The effects in the $\Delta kaiAB1C1$ mutant are similar but smaller. This can be mainly explained by RpaA function in transcriptional regulation even in the absence of Kai-controlled phosphorylation. Phenotypic analyses of phosphor-mimicking variants of RpaA could be helpful to evaluate this hypothesis in future studies. Further, the lack of RpaA-RpaB interactions in the $\Delta rpaA$ mutant might affect the control of the large RpaB-dependent regulon, which partially overlaps with the RpaA regulon (e.g., control of the *psaAB* operon) (Seino et al., 2009; Köbler et al., 2018). Moreover, a recent study by Riediger et al. (2019) largely extended the RpaB regulon, which currently includes many enzymes involved in primary carbon and nitrogen metabolism, likely contributing to the larger impact of RpaA deficiency on L/D-mediated metabolic changes. In addition, or alternatively, the presence of the likely only partially neofunctionalized KaiB3C3 and KaiB2C2 systems in *Synechocystis* could compensate for the loss of the KaiAB1C1 complex. At least for the KaiC3-based system, it has been shown

that it interacts with the KaiAB1C1 complex and modulates its function (Wiegard et al., 2020).

It has been suggested that the NADPH/NADP ratio plays a major role in the diurnal growth of *Synechocystis* (Saha et al., 2016). This ratio is known as the main redox signal and has a pronounced impact on enzyme activities in the CBB cycle, glycolysis and gluconeogenesis. For example, the NADPH/NADP ratio switches the activities of the CBB enzymes Gap2 and Prk on and off via the small redox-sensitive protein CP12 in L to D transitions (McFarlane et al., 2019). Hence, the tendency of higher NADPH/NADP ratios in the mutants, especially in $\Delta rpaA$, suggests that these and other metabolic redox cofactors likely contribute to the observed disbalanced carbon and nitrogen metabolism in L/D transitions. Moreover, the continued and enhanced activity of RubisCO in D leads to the observed accumulation of 2PG in both mutants due to the enhanced oxygenase reaction in the presence of lower $C_i/O_2$ ratios in D. 2PG can be toxic and provides a metabolic signal that falsely indicates carbon limitation. 2PG accumulation in $\Delta rpaA$ is much more pronounced than that in $\Delta kaiAB1C1$, explaining the previously detected overexpression of transcripts involved in $C_i$ limitation response in $\Delta rpaA$ (Köbler et al., 2018). The PHB deficiency observed in both strains can be traced to the lower accumulation of mRNAs encoding the enzymes involved in PHB synthesis. Furthermore, this deficiency might be caused by the lower pyruvate pool and respective metabolic limitation of the acetyl-CoA precursor of PHB synthesis in both mutants. However, the lack of PHB should not affect the growth of cells in L/D cycles as shown by Damrow et al. (2016), suggesting that this deficiency is not the primary cause of the phenotype of the analyzed mutants.

Moreover, previous analyses showed that mixotrophic conditions, i.e., feeding glucose in the L, have an aggravating effect on the growth of both mutant strains in L/D cycles (Dörrich et al., 2014; Köbler et al., 2018). The $\Delta rpaA$ and $\Delta kaiABC$ mutants showed impaired growth only under diurnal conditions, while a 12 or 48 h incubation in D followed by continuous light did not affect the growth of the mutants (**Supplementary Figure 6**; Köbler et al., 2018). These findings indicate a failure of the $\Delta rpaA$ and $\Delta kaiABC$ mutants to adapt to diurnal light changes, rather than a lack of circadian regulation which should have been be induced after a synchronization with D incubation. Similar to these results, Beck et al. (2014) showed transcript oscillations in *Synechocystis* only during cultivation in L/D cycles, which stopped after transfer to constant L or D conditions. Thus, the presence of a true circadian system in *Synechocystis* remains inconclusive, whereas a diurnal regulation of transcription and metabolism seems to be likely. In the present study, we provide evidence suggesting that high $CO_2$ supplementation improves the ability of both mutants to grow at diurnal L/D cycles. In contrast, glucose addition and limiting $C_i$ availability result in redox imbalance. Therefore, the defect in the mutants' ability to grow diurnally is likely associated with disturbed redox homeostasis as previously shown in *Synechococcus elongatus* PCC 7942 (Diamond et al., 2017). The redox imbalance in the two mutants is also reflected by

the transcriptional changes as genes encoding flavoproteins (Flv), especially Flv2 and Flv4, are significantly upregulated compared to those in the wild type (Köbler et al., 2018). These flavoproteins along with Flv1 and Flv3 are required for the Mehler-like reaction in *Synechocystis* to support growth under fluctuating or high light conditions (Santana-Sanchez et al., 2019).

Finally, motivated by the potential of *Synechocystis* and other cyanobacteria for biotechnological applications and the important role of the circadian clock in controlling cyanobacterial metabolism, several groups utilized deletion and overproduction strains of the SasA-RpaA output module and resulting analyzed metabolic changes. Most importantly, the overexpression of *sasA* and *rpaA* resulted in enhanced sugar catabolism in the D (Iijima et al., 2015; Osanai et al., 2015). Our analysis of a mutant lacking the *rpaA* gene reveals the opposite effects, i.e., more carbon is exported from the CBB cycle into lower glycolysis and TCA cycle, which is consistent with published data of *rpaA* overexpression (Iijima et al., 2015). Hence, the results presented here and by other groups provide evidence suggesting that an intact KaiAB1C1-based system is required in *Synechocystis* for the improved production of C-based metabolites under natural L/D cycles with cyanobacteria.

## DATA AVAILABILITY STATEMENT

The original contributions presented in the study are included in the article/**Supplementary Material**, further inquiries can be directed to the corresponding author/s.

## AUTHOR CONTRIBUTIONS

## FUNDING

## ACKNOWLEDGMENTS

## SUPPLEMENTARY MATERIAL

The Supplementary Material for this article can be found online at: https://www.frontiersin.org/articles/10.3389/fpls.2021.675227/full#supplementary-material

## REFERENCES

Beck, C., Hertel, S., Rediger, A., Lehmann, R., Wiegard, A., Kölsch, A., et al. (2014). Daily expression pattern of protein-encoding genes and small noncoding RNAs in *Synechocystis* sp. strain PCC 6803. *Appl. Environ. Microbiol.* 80, 5195–5206. doi: 10.1128/AEM.01086-14

Chen, X., Schreiber, K., Appel, J., Makowka, A., Fähnrich, B., Roettger, M., et al. (2016). The Entner–Doudoroff pathway is an overlooked glycolytic route in cyanobacteria and plants. *Proc. Natl. Acad. Sci. U.S.A.* 113, 5441–5446. doi: 10.1073/pnas.1521916113

Ciebiada, M., Kubiak, K., and Daroch, M. (2020). Modifying the cyanobacterial metabolism as a key to efficient biopolymer production in photosynthetic microorganisms. *Int. J. Mol. Sci.* 21:7204. doi: 10.3390/ijms21197204

Cohen, S. E., and Golden, S. S. (2015). Circadian rhythms in Cyanobacteria. *Microbiol. Mol. Biol. Rev.* 79, 373–385. doi: 10.1128/MMBR. 00036-15

Damrow, R., Maldener, I., and Zilliges, Y. (2016). The multiple functions of common microbial carbon polymers, glycogen and PHB, during stress responses in the non-diazotrophic cyanobacterium *Synechocystis* sp. PCC 6803. *Front. Microbiol.* 7:966. doi: 10.3389/fmicb.2016.00966

Diamond, S., Rubin, B. E., Shultzaberger, R. K., Chen, Y., Barber, C. D., and Golden, S. S. (2017). Redox crisis underlies conditional light–dark lethality in cyanobacterial mutants that lack the circadian regulator, RpaA. *Proc. Natl. Acad. Sci. U.S.A.* 114, E580–E589. doi: 10.1073/pnas.1613078114

Dienst, D., Dühring, U., Mollenkopf, H. J., Vogel, J., Golecki, J., Hess, W. R., et al. (2008). The cyanobacterial homologue of the RNA chaperone Hfq is essential for motility of *Synechocystis* sp. PCC 6803. *Microbiology* 154, 3134–3143. doi: 10.1099/mic.0.2008/020222-0

Dörrich, A. K., Mitschke, J., Siadat, O., and Wilde, A. (2014). Deletion of the *Synechocystis* sp. PCC 6803 *kaiAB1C1* gene cluster causes impaired cell growth under light–dark conditions. *Microbiology* 160, 2538–2550. doi: 10.1099/mic.0.081695-0

Dvornyk, V., Vinogradova, O., and Nevo, E. (2002). Long-term microclimatic stress causes rapid adaptive radiation of *kaiABC* clock gene family in a cyanobacterium, *Nostoc linckia*, from "Evolution Canyons" I and II, Israel. *Proc. Natl. Acad. Sci. U.S.A.* 99, 2082–2087. doi: 10.1073/pnas.261699498

Eisenhut, M., Ruth, W., Haimovich, M., Bauwe, H., Kaplan, A., and Hagemann, M. (2008). The photorespiratory glycolate metabolism is essential for cyanobacteria and might have been conveyed endosymbiontically to plants. *Proc. Natl. Acad. Sci. U.S.A.* 105, 17199–17204. doi: 10.1073/pnas.0807043105

Erban, A., Martinez-Seidel, F., Rajarathinam, Y., Dethloff, F., Orf, I., Fehrle, I., et al. (2020). "Multiplexed profiling and data processing methods to identify temperature-regulated using gas chromatography coupled to mass spectrometry," in *Plant cold acclimation: Methods in Molecular Biology (Methods and Protocols),* eds D. K. Hincha and E. Zuther (Totowa, NJ: Humana Press), 203–239. doi: 10.1007/978-1-0716-0660-5_15

Flügel, F., Timm, S., Arrivault, S., Florian, A., Stitt, M., Fernie, A. R., et al. (2017). The photorespiratory metabolite 2-phosphoglycolate regulates photosynthesis and starch accumulation in Arabidopsis. *Plant Cell* 29, 2537–2551. doi: 10.1105/tpc.17.00256

Gutu, A., and O'Shea, E. K. (2013). Two antagonistic clock-regulated histidine kinases time the activation of circadian gene expression. *Mol. Cell* 50, 288–294. doi: 10.1016/j.molcel.2013.02.022

Huege, J., Goetze, J., Schwarz, D., Bauwe, H., Hagemann, M., and Kopka, J. (2011). Modulation of the major paths of carbon in photorespiratory mutants of *Synechocystis. PLoS ONE* 6:e16278. doi: 10.1371/journal.pone.0016278

Iijima, H., Shirai, T., Okamoto, M., Kondo, A., Hirai, M. Y., and Osanai, T. (2015). Changes in primary metabolism under light and dark conditions in response to overproduction of a response regulator RpaA in the unicellular cyanobacterium Synechocystis sp. PCC 6803. Front. Microbiol. 6:888. doi: 10.3389/fmicb.2015.00888

Ishiura, M., Kutsuna, S., Aoki, S., Iwasaki, H., Andersson, C. R., Tanabe, A., et al. (1998). Expression of a gene cluster kaiABC as a circadian feedback process in cyanobacteria. Science 281, 1519–1523. doi: 10.1126/science.281.53 82.1519

Iwasaki, H., Taniguchi, Y., Ishiura, M., and Kondo, T. (1999). Physical interactions among circadian clock proteins KaiA, KaiB and KaiC in cyanobacteria. EMBO J. 18, 1137–1145. doi: 10.1093/emboj/18.5.1137

Jiang, Y. L., Wang, X. P., Sun, H., Han, S. J., Li, W. F., Cui, N., et al. (2018). Coordinating carbon and nitrogen metabolic signaling through the cyanobacterial global repressor NdhR. Proc. Natl. Acad. Sci. U.S.A. 115, 403–408. doi: 10.1073/pnas.1716062115

Kirsch, F., Klähn, S., and Hagemann, M. (2019). Salt-regulated accumulation of the compatible solutes sucrose and glucosylglycerol in cyanobacteria and its biotechnological potential. Front. Microbiol. 10:2139. doi: 10.3389/fmicb.2019.02139

Köbler, C., Schultz, S. J., Kopp, D., Voigt, K., and Wilde, A. (2018). The role of the Synechocystis sp. PCC 6803 homolog of the circadian clock output regulator RpaA in day-night transitions. Mol. Microbiol. 110, 847–861. doi: 10.1111/mmi.14129

Koch, M., Berendzen, K. W., and Forchhammer, A. K. (2020a). On the role and production of polyhydroxybutyrate (PHB) in the cyanobacterium Synechocystis sp. PCC 6803. Life 10:47. doi: 10.3390/life10040047

Koch, M., Doello, S., Gutekunst, K., and Forchhammer, K. (2019). PHB is produced from glycogen turn-over during nitrogen starvation in Synechocystis sp. PCC 6803. Int. J. Mol. Sci. 20:1942. doi: 10.3390/ijms20081942

Koch, M., and Forchhammer, K. (2021). Polyhydroxybutyrate: a useful product of chlorotic cyanobacteria. Microb. Physiol. doi: 10.1159/000515617. [Epub ahead of print].

Koch, M., Orthwein, T., Alford, J. T., and Forchhammer, K. (2020b). The Slr0058 protein from Synechocystis sp. PCC 6803 is a novel regulatory protein involved in PHB granule formation. Front. Microbiol. 11:809. doi: 10.3389/fmicb.2020.00809

Kopka, J., Schauer, N., Krueger, S., Birkemeyer, C., Usadel, B., Bergmuller, E., et al. (2005). GMD@CSB.DB: the golm metabolome database. Bioinformatics 21, 1635–1638. doi: 10.1093/bioinformatics/bti236

Kopka, J., Schmidt, S., Dethloff, F., Pade, N., Berendt, S., Schottkowski, M., et al. (2017). Systems analysis of ethanol production in the genetically engineered cyanobacterium Synechococcus sp. PCC 7002. Biotechnol. Biofuels 10:56. doi: 10.1186/s13068-017-0741-0

Luedemann, A., Strassburg, K., Erban, A., and Kopka, J. (2008). TagFinder for the quantitative analysis of gas chromatography—mass spectrometry (GC-MS)-based metabolite profiling experiments. Bioinformatics 24, 732–737. doi: 10.1093/bioinformatics/btn023

Makowka, A., Nichelmann, L., Schulze, D., Spengler, K., Wittmann, C., Forchhammer, K., et al. (2020). Glycolytic shunts replenish the Calvin – Benson – Bassham Cycle as anaplerotic reactions in cyanobacteria. Mol. Plant 13, 471–482. doi: 10.1016/j.molp.2020.02.002

Markson, J. S., Piechura, J. R., Puszynska, A. M., and O'Shea, E. K. (2013). Circadian control of global gene expression by the cyanobacterial master regulator RpaA. Cell 155, 1396–1408. doi: 10.1016/j.cell.2013. 11.005

McFarlane, C. R., Shah, N. R., Kabasakal, B. V., Echeverria, B., Cotton, C. A. R., Bubeck, D., et al. (2019). Structural basis of light-induced redox regulation in the Calvin–Benson cycle in cyanobacteria. Proc. Natl. Acad. Sci. U.S.A. 116, 20984–20990. doi: 10.1073/pnas.1906722116

Miller, S. R., Wood, A. M., Blankenship, R. E., Kim, M., and Ferriera, S. (2011). Dynamics of gene duplication in the genomes of chlorophyll d-producing cyanobacteria: Implications for the ecological niche. Genome Biol. Evol. 3, 601–613. doi: 10.1093/gbe/evr060

Nishimura, T., Takahashi, Y., Yamaguchi, O., Suzuki, H., Maeda, S., and Omata, T. (2008). Mechanism of low $CO_2$-induced activation of the cmp

bicarbonate transporter operon by a LysR family protein in the cyanobacterium Synechococcus elongatus strain PCC 7942. Mol. Microbiol. 68, 98–109. doi: 10.1111/j.1365-2958.2008.06137.x

Orf, I., Klähn, S., Schwarz, D., Frank, M., Hess, W. R., Hagemann, M., et al. (2015). Integrated analysis of engineered carbon limitation in a quadruple $CO_2$/$HCO_3^-$-uptake mutant of Synechocystis sp. PCC 6803. Plant Physiol. 169, 1787–1806. doi: 10.1104/pp.15.01289

Orthwein, T., Scholl, J., Spät, P., Lucius, S., Koch, M., Macek, B., et al. (2021). The novel PII -interactor PirC identifies phosphoglycerate mutase as key control point of carbon storage metabolism in cyanobacteria. Proc. Natl. Acad. Sci. U.S.A. 118:e2019988118. doi: 10.1073/pnas.2019988118

Osanai, T., Shirai, T., Iijima, H., Kuwahara, A., Suzuki, I., Kondo, A., et al. (2015). Alteration of cyanobacterial sugar and amino acid metabolism by overexpression hik8, encoding a KaiC-associated histidine kinase. Environ. Microbiol. 17, 2430–2440. doi: 10.1111/1462-2920.12715

Panda, B., Jain, P., Sharma, L., and Mallick, N. (2006). Optimization of cultural and nutritional conditions for accumulation of poly-β-hydroxybutyrate in Synechocystis sp. PCC 6803. Bioresour. Technol. 97, 1296–1301. doi: 10.1016/j.biortech.2005.05.013

Pinto, F., Thapper, A., Sontheim, W., and Lindblad, P. (2009). Analysis of current and alternative phenol based RNA extraction methodologies for cyanobacteria. BMC Mol. Biol. 10:79. doi: 10.1186/1471-2199-10-79

Puszynska, A. M., and O'Shea, E. K. (2017). Switching of metabolic programs in response to light availability is an essential function of the cyanobacterial circadian output pathway. Elife 6:e23210. doi: 10.7554/eLife.23210

Rai, S., Lucius, S., Kern, R., Bauwe, H., Kaplan, A., Kopka, J., et al. (2018). The Synechocystis sp. PCC 6803 genome encodes up to four 2-phosphoglycolate phosphatases. Front. Plant Sci. 9:1718. doi: 10.3389/fpls.2018.01718

Riediger, M., Kadowaki, T., Nagayama, R., Georg, J., Hihara, Y., and Hess, W. R. (2019). Biocomputational analyses and experimental validation identify the regulon controlled by the redox-responsive transcription factor RpaB. iScience 15, 316–331. doi: 10.1016/j.isci.2019.04.033

Rippka, R., Deruelles, J., Herdman, M., Waterbury, J. B., and Stanier, R. (1979). Generic assignments, strain histories and properties of pure cultures of cyanobacteria. Microbiology 111, 1–61. doi: 10.1099/00221287-111-1-1

Saha, R., Liu, D., Connor, A. H., Liberton, M., Yu, J., and Bhattacharyya-Pakrasi, M. (2016). Diurnal regulation of cellular processes in the cyanobacterium Synechocystis sp. strain PCC 6803: Insights from transcriptomic, fluxomic, and physiological analyses. mBio 7, e00464–e00416. doi: 10.1128/mBio.00464-16

Santana-Sanchez, A., Solymosi, D., Mustila, H., Bersanini, L., Aro, E. M., and Allahverdiyeva, Y. (2019). Flavodiiron proteins 1-to-4 function in versatile combinations in $O_2$ photoreduction in cyanobacteria. Elife 8:e45766. doi: 10.7554/eLife.45766

Seino, Y., Takahashi, T., and Hihara, Y. (2009). The response regulator RpaB binds to the upstream element of Photosystem I genes to work for positive regulation under low-light conditions in Synechocystis sp. Strain PCC 6803. J. Bacteriol. 191, 1581–1586. doi: 10.1128/JB.01588-08

Shibata, M., Katoh, H., Sonoda, M., Ohkawa, H., Shimoyama, M., Fukuzawa, H., et al. (2002). Genes essential to sodium-dependent bicarbonate transport in cyanobacteria. J. Biol. Chem. 277, 18658–18664. doi: 10.1074/jbc. M112468200

Shibata, M., Ohkawa, H., Kaneko, T., Fukuzawa, H., Tabata, S., Kaplan, A., et al. (2001). Distinct constitutive and low-$CO_2$-induced $CO_2$ uptake systems in cyanobacteria: genes involved and their phylogenetic relationship with homologous genes in other organisms. Proc. Natl. Acad. Sci. U.S.A. 98, 11789–11794. doi: 10.1073/pnas.191258298

Tamoi, M., Miyazaki, T., Fukamizo, T., and Shigeoka, S. (2005). The Calvin cycle in cyanobacteria is regulated by CP12 via the NAD(H)/NADP(H) ratio under light/dark conditions. Plant J. 42, 504–513. doi: 10.1111/j.1365-313X.2005.02391.x

Taroncher-Oldenburg, G., Nishina, K., and Stephanopoulos, G. (2000). Identification and analysis of the polyhydroxyalkanoate-specific β-ketothiolase and acetoacetyl coenzyme A reductase genes in the cyanobacterium Synechocystis sp. strain PCC6803. Appl. Environ. Microbiol. 66, 4440–4448. doi: 10.1128/AEM.66.10.4440-4448.2000

Trautmann, D., Vo,ß, B., Wilde, A., Al-Babili, S., and Hess, W. R. (2012). Microevolution in cyanobacteria: Re-sequencing a motile substrain of

*Synechocystis* sp. PCC 6803. *DNA Res.* 19, 435–448. doi: 10.1093/dnares/dss024

Weissenbach, J., Ilhan, J., Bogumil, D., Hülter, N., Stucken, K., and Dagan, T. (2017). Evolution of chaperonin gene duplication in Stigonematalean Cyanobacteria (Subsection V). *Genome Biol. Evol.* 9:evw287. doi: 10.1093/gbe/evw287

Werner, A., Broeckling, C. D., Prasad, A., and Peebles, C. A. M. (2019). A comprehensive time-course metabolite profiling of the model cyanobacterium *Synechocystis* sp. PCC 6803 under diurnal light:dark cycles. *Plant J.* 99, 379–388. doi: 10.1111/tpj.14320

Wiegard, A., Dörrich, A. K., Deinzer, H. T., Beck, C., Wilde, A., Holtzendorff, J., et al. (2013). Biochemical analysis of three putative KaiC clock proteins from *Synechocystis* sp. PCC 6803 suggests their functional divergence. *Microbiology* 159, 948–958. doi: 10.1099/mic.0.065425-0

Wiegard, A., Köbler, C., Oyama, K., Dörrich, A. K., Azai, C., Terauchi, K., et al. (2020). *Synechocystis* KaiC3 displays temperature- and KaiB-dependent ATPase activity and is important for growth in darkness. *J. Bacteriol.* 202, e00478–e00419. doi: 10.1128/JB.00478-19

Xiong, W., Brune, D., and Vermaas, W. F. (2014). The γ-aminobutyric acid shunt contributes to closing the tricarboxylic acid cycle in *Synechocystis* sp. PCC 6803. *Mol. Microbiol.* 93, 786–796. doi: 10.1111/mmi.12699

Xu, M., Bernát, G., Singh, A., Mi, H., Rögner, M., Pakrasi, H. B., et al. (2008). Properties of mutants of *Synechocystis* sp. strain PCC 6803 lacking inorganic carbon sequestration systems. *Plant Cell Physiol.* 49, 1672–1677. doi: 10.1093/pcp/pcn139

Zhang, S., and Bryant, D. A. (2011). The tricarboxylic acid cycle in cyanobacteria. *Science* 334, 1551–1553. doi: 10.1126/science.1210858

Zhang, Y., Krahnert, I., Bolze, A., Gibon, Y., and Fernie, A. R. (2020). Adenine nucleotide and nicotinamide adenine dinucleotide measurements in plants. *Curr. Protoc. Plant Biol.* 5:e20115. doi: 10.1002/cppb.20115